

On the sealing and lubrication mechanism of radial lip seals

Citation for published version (APA):

Stakenborg, M. J. L. (1988). *On the sealing and lubrication mechanism of radial lip seals*. [Phd Thesis 1 (Research TU/e / Graduation TU/e), Mechanical Engineering]. Technische Universiteit Eindhoven.
<https://doi.org/10.6100/IR291319>

DOI:

[10.6100/IR291319](https://doi.org/10.6100/IR291319)

Document status and date:

Published: 01/01/1988

Document Version:

Publisher's PDF, also known as Version of Record (includes final page, issue and volume numbers)

Please check the document version of this publication:

- A submitted manuscript is the version of the article upon submission and before peer-review. There can be important differences between the submitted version and the official published version of record. People interested in the research are advised to contact the author for the final version of the publication, or visit the DOI to the publisher's website.
- The final author version and the galley proof are versions of the publication after peer review.
- The final published version features the final layout of the paper including the volume, issue and page numbers.

[Link to publication](#)

General rights

Copyright and moral rights for the publications made accessible in the public portal are retained by the authors and/or other copyright owners and it is a condition of accessing publications that users recognise and abide by the legal requirements associated with these rights.

- Users may download and print one copy of any publication from the public portal for the purpose of private study or research.
- You may not further distribute the material or use it for any profit-making activity or commercial gain
- You may freely distribute the URL identifying the publication in the public portal.

If the publication is distributed under the terms of Article 25fa of the Dutch Copyright Act, indicated by the "Taverne" license above, please follow below link for the End User Agreement:

www.tue.nl/taverne

Take down policy

If you believe that this document breaches copyright please contact us at:

openaccess@tue.nl

providing details and we will investigate your claim.

ON THE
SEALING AND LUBRICATION MECHANISM
OF
RADIAL LIP SEALS

M.J.L. STAKENBORG

ON THE SEALING AND
LUBRICATION MECHANISM OF RADIAL LIP SEALS

ON THE
SEALING AND LUBRICATION MECHANISM
OF
RADIAL LIP SEALS

PROEFSCHRIFT

TER VERKRIJGING VAN DE GRAAD VAN DOCTOR AAN
DE TECHNISCHE UNIVERSITEIT EINDHOVEN, OP GEZAG
VAN DE RECTOR MAGNIFICUS, PROF. IR. M. TELS, VOOR
EEN COMMISSIE AANGEWEEZEN DOOR HET COLLEGE VAN
DEKANEN IN HET OPENBAAR TE VERDEDIGEN OP
DINSDAG 20 SEPTEMBER 1988 TE 14.00 UUR

DOOR

MARCEL JOS LOU STAKENBORG

GEBOREN TE TORONTO (CANADA)

DIT PROEFSCHRIFT IS GOEDGEKEURD
DOOR DE PROMOTOR:

PROF. DR. IR. M.J.W. SCHOUTEN

Ter nagedachtenis aan Frans Mulders.

CONTENTS

SUMMARY.

SAMENVATTING (In Dutch).

NOMENCLATURE.

CHAPTER 1 : Introduction.

- 1.1 Radial lip seals.
- 1.2 Optimization.
- 1.3 State of the art.
- 1.4 Objective of this study.
- 1.5 Complications in seal research.
- 1.6 Outline of this thesis.
- 1.7 General remarks.
- 1.8 References.

CHAPTER 2 : The sealing mechanism, measurements and observations.

- 2.1 Introduction.
- 2.2 The test-rig.
- 2.3 Observations using the glassfibre test-rig.
- 2.4 Discussion of the observations.
- 2.5 Drop in pressure over the oil-air interface.
- 2.6 Summary.
- 2.7 References.

CHAPTER 3 : The seal-shaft contact: static, isothermal conditions.

- 3.1 Introduction.
- 3.2 Material Characterisation.
- 3.3 FEM model definition.
- 3.4 Discussion of the FEM results.
- 3.5 Rubber swelling.
- 3.6 Centrifugal forces.
- 3.7 Summary.
- 3.8 References.

CHAPTER 4 : The seal-shaft contact: static, non-isothermal conditions.

- 4.1 Introduction.
- 4.2 Temperature effects.
- 4.3 Temperature distribution in the seal.
- 4.4 Influence of temperature on the contact conditions.
- 4.5 Discussion of the results.
- 4.6 Summary.
- 4.7 References.

CHAPTER 5 : Contact temperature.

- 5.1 Introduction.
- 5.2 Thermal network model.
- 5.3 Measuring the contact temperature.
- 5.4 Numerical results.
- 5.5 Summary.
- 5.6 References.

CHAPTER 6 : The pumping mechanism, a model.

- 6.1 Introduction.
- 6.2 Principles of the visco-seal concept.
- 6.3 Model definition.
- 6.4 Discretization of the problem.
- 6.5 Discussion of the results.
- 6.6 Summary.
- 6.6 References.

CHAPTER 7 : Leakage, a model.

- 7.1 Introduction.
- 7.2 Model definition.
- 7.3 Numerical results.
- 7.4 Summary.
- 7.5 References.

CHAPTER 8 : Visco-elastohydrodynamic lubrication.

- 8.1 Introduction.
- 8.2 Dynamic behaviour of rubber.
- 8.3 Dynamic behaviour of the seal.
- 8.4 FEM model of the seal.
- 8.5 Transfer function of the seal.
- 8.6 Interaction between fluid film and viscoelastic seal.
- 8.7 Discussion.
- 8.8 conclusions.
- 8.9 References.

CHAPTER 9 : Final remarks.

- 9.1 Practical utility of this study.
- 9.2 Main conclusions.
- 9.3 Future research.

APPENDICES :

- A1 Calculation of the pressure drop over the oil-air interface.
- A2 A leakage model for radial lip seals.
- A3 Physical properties for the dynamic FEM model.

DANKWOORD.

CURRICULUM VITAE.

SUMMARY

Radial lip seals are frequently used in machinery to seal rotating shafts at low oil pressures. The functioning of radial lip seals is based on the formation of a sealing and lubricating oilfilm between the seal lip and the shaft surface. The sealing mechanism and lubrication mechanism are complex and poorly understood. The aim of this study is to gain a better insight into both mechanisms.

The sealing mechanism was observed experimentally using a bundle of glassfibres fixed in the seal-shaft contact area. It was found that the sealing mechanism is based on an active pumping action of the seal, counterbalanced by capillary suction forces of the oil-air interface on the air-side of the seal. Above a certain angular velocity cavitation occurs in the contact area, starting on the edges of the contact area.

The friction heat generated in the contact area results in a raise in seal lip temperature. Investigating the sealing and lubrication mechanism it is important to know the influence of temperature on the contact conditions. The influence of temperature effects on the contact conditions is studied, using a coupled temperature-stress finite element method (FEM) analysis.

A numerical model is presented to calculate the seal-shaft contact temperature for both transient and steady-state situations. This numerical model is based on the thermal network method, where a machine is divided into thermal components such as heat resistors, capacitors and sources. Three different experimental techniques: NTC thermistors, thin film microtransducers and infra-red measurements were used to measure the contact temperature.

On basis of the visco-seal principle a model is derived which describes the active pumping action of radial lip seals.

A model is formulated which describes leakage at higher shaft angular velocities in consequence of a breakdown of the oil-air interface on the air-side of the seal, due to centrifugal forces acting on the oil.

In practice a dynamic excitation of the seal lip occurs due to out of roundness of the shaft or motions of the shaft center. The influence of a dynamic excitation of the seal lip is studied using a dynamic FEM analysis. The interaction between the visco-elastic and inertial seal lip and the lubricating fluid film is investigated. It is shown how viscous and inertial effects can lead to a phenomenon which is designated as visco-elastohydrodynamic (VEHD) lubrication.

SAMENVATTING.

Radiale lipafdichtingen worden veelvuldig toegepast in de werktuigbouw om roterende assen af te dichten bij lage oliedrukken. De werking van deze afdichtingen is gebaseerd op the vorming van een afdichtende en smerende oliefilm tussen de afdichtingslip en de as. Het afdicht- en het smeringsmechanisme zijn complex en nog niet goed doorgrond. Het doel van deze studie is een beter inzicht te krijgen in beide mechanismen.

Het afdichtmechanisme werd onderzocht m.b.v. een bundel glasfibers in de contactzone tussen as en afdichting. Daarbij bleek dat het afdichtmechanisme is gebaseerd op een actieve pompwerking die wordt gecompenseerd door capillaire zuigkrachten van de meniscus aan de luchtzijde van de afdichting. Boven een bepaalde hoeksnelheid trad cavitatie op, die begon aan de randen van de contactzone.

De in de contact zone gedissipeerde wrijvingswarmte resulteert in een temperatuurstijging van de afdichtings lip. Bij een onderzoek naar het afdicht- en het smeringsmechanisme is kennis van de invloed van de temperatuur op de contactcondities van belang. De invloed van de temperatuur op de contactcondities wordt onderzocht m.b.v. een gekoppelde temperatuur-spannings berekening met de eindige elementen methode (EEM).

Er wordt een numeriek model geïntroduceerd voor de berekening van de contacttemperatuur voor stationaire en instationaire situaties. Dit model is gebaseerd op de thermische netwerk methode, waarbij een machine wordt verdeeld in thermische componenten zoals warmteweerstanden, capaciteiten en bronnen. Drie verschillende experimentele technieken (NTC thermistors, dunne film signaalopnemers en infra-rood metingen) zijn toegepast bij de bepaling van de contacttemperatuur.

Op basis van het visco-seal principe, wordt een model afgeleid voor de beschrijving van het pomp mechanisme van radiale lipafdichtingen.

Er wordt een model geformuleerd voor de beschrijving van lekkage bij hogere as hoeksnelheden, die ontstaat t.g.v. het in elkaar klappen van de meniscus aan de luchtzijde van de afdichting, onder invloed van centrifugale krachten op de olie.

In praktijksituaties ontstaat er een dynamische excitatie van de afdichtingslip t.g.v. onrondheid of excentriciteit van de as. De invloed van een dynamische excitatie van de afdichtingslip wordt onderzocht m.b.v. een dynamische EEM analyse. De interactie tussen de visco-elastische- en massastraagheids eigenschappen van de afdichting en de smeerfilm wordt onderzocht. Er wordt aangetoond hoe viskeuze- en massastraagheidseffecten kunnen leiden tot een fenomeen dat aangeduid wordt met de naam visco-elastohydrodynamische (VEHD) smering.

NOMENCLATURE

a	Width of ridge	[m]
b	Contact width	[m]
c	Specific heat	[J/kg.K]
c	Height of groove	[m]
d_1	Diameter shaft	[m]
d_2	Diameter unloaded seal	[m]
e	Eccentricity between C_{se} and C_{sh}	[m]
e	Width of groove	[m]
f	Frequency	[1/s]
f	Friction coefficient	[-]
f_s	Shaft rotational frequency	[1/s]
f_w	Whirl frequency	[1/s]
$h(t, \xi)$	Impuls response function	[Pa/m.s]
h_{air}	Convective film coefficient to air	[W/m.K]
h_{oil}	Convective film coefficient to oil	[W/m.K]
h	Gap heighth	[m]
\bar{h}	Average film heighth	[m]
l	Length	[m]
m_{spr}	Mass of garter spring	[kg]
p	Pressure	[Pa]
p_0	Contact pressure	[Pa]
p_0	Fluid film pressure	[Pa]
$p(t, \xi)$	Contact stress in time domain	[Pa]
$p_d(t, \xi)$	Dynamic component of contact stress	[Pa]
$ p_d $	Amplitude of $p_d(t, \xi)$	[Pa]
$p_s(\xi)$	Static component of contact stress	[Pa]
$p_t(t, \xi)$	Total contact stress	[Pa]
p_v	Vapour pressure	[Pa]
q	Heat flux	[W/m ²]
s	gap heighth	[m]
t	Time	[s]
v	Tangetial displacement field	[m]
\vec{v}	Displacement vector	[m]
x(t)	Input signal in time domain	[m]
$x_d(t)$	Sinusoidal displacement signal	[m]
$ x_d $	Amplitude of $x_d(t)$	[m]
$z(t, \xi)$	Displacement signal of the lip	[m]
C_{se}	Geometric center of the seal	[-]
C_{sh}	Geometric center of the shaft	[-]
C_1, C_2	Mooney constants	[Pa]
E	E-modulus	[Pa]
F(-)	Complex forward Fourier transform	[-]

F_r	Radial contact force	[N]
F_{r1}	Radial lip force	[N]
F_{r2}	Radial garter spring force	[N]
F_T	Nodal force vector	[N]
$G(t)$	Stress relaxation function	[Pa]
$H(f, \xi)$	Transfer function in frequency domain	[Pa/m]
K_T	tangential stiffness matrix	[N/m]
$P(f, \xi)$	Contact pressure in frequency domain	[Pa.s]
R	Shaft radius	[m]
R_i	Radius of interface	[m]
R_i	Thermal resistor i	[K/W]
T	Torque	[N.m]
T	Temperature	[°C]
T	Period time	[s]
T_c	Contact temperature	[°C]
T_m	Measured torque	[N.m]
W	Strain energy function	[-]
$X(f, \xi)$	Input signal in frequency domain	[m.s]
α	Thermal expansion coefficient	[1/K]
α_1	Wetting angle oil-steel	[rad]
α_2	Wetting angle oil-rubber	[rad]
δ	Interference	[m]
ξ	Axial coordinate in contact area	[m]
ϕ	Phase shift angle	[rad]
$\phi(x)$	Groove angle	[rad]
σ_{rr}	Principal stress in radial direction	[Pa]
σ_{vm}	Von Mises stress	[Pa]
γ	Surface tension oil	[N/m]
η	Dynamic viscosity	[Pa.s]
λ	Thermal conductivity	[W/m.K]
λ	Stretch ratio	[-]
ρ	Specific mass	[kg/m ³]
τ_i	relaxation time constant	[s]
ω_s	Shaft angular velocity	[rad/s]
ω_w	Whirl angular velocity	[rad/s]
ω_1	Shaft angular velocity	[rad/s]
ω_2	Seal angular velocity	[rad/s]
τ	Shear stress distribution	[Pa]
Δp	Pumping pressure	[Pa]
Γ_i	Boundary i	[-]

CHAPTER 1 : INTRODUCTION.

1.0 OVERVIEW.

- 1.1 Radial lip seals.
- 1.2 Optimization.
- 1.3 State of the art.
- 1.4 Objective of this study.
- 1.5 Complications in seal research.
- 1.6 Outline of this thesis.
- 1.7 General remarks.
- 1.8 References.

The sealing mechanism and lubrication mechanism of radial lip seals are complex and poorly understood tribological processes, governed by many parameters. To come to an optimization of these seals a better understanding is necessary. The aim of this study is to get a better insight into the sealing and the lubrication mechanism.

1.1 RADIAL LIP SEALS.

Radial lip seals are frequently used in machinery to seal rotating shafts at low oil pressures, and to prevent the penetration of dust, dirt or water from the outside. These relatively simple construction elements exhibit a remarkable sealing performance and service life. The functioning of these seals is based on the formation of a thin sealing and lubricating oilfilm between the seal lip and the rotating shaft.

The geometry of radial lip seals is the result of a long trial-and-error process. The geometrical shape of radial lip seals is standardized, e.g. in DIN 3760 (German Industrial Standard). A standard radial lip seal generally consists of a stiff part (a molded synthetic rubber body reinforced with a metallic case) and a flexible part (a molded synthetic rubber seal lip with a garter spring), see figure 1.1

A difference in outer diameter d_1 of the shaft and inner diameter d_2 of the seal, referred to as the interference δ (where $\delta = d_1 - d_2$ and $d_1 > d_2$), results in a radial contact force F_r after mounting the seal on the shaft. This contact force F_r is the sum of a force F_{r1} due to elastic deformation of the lip and a force F_{r2} caused by elongation of the garter spring.

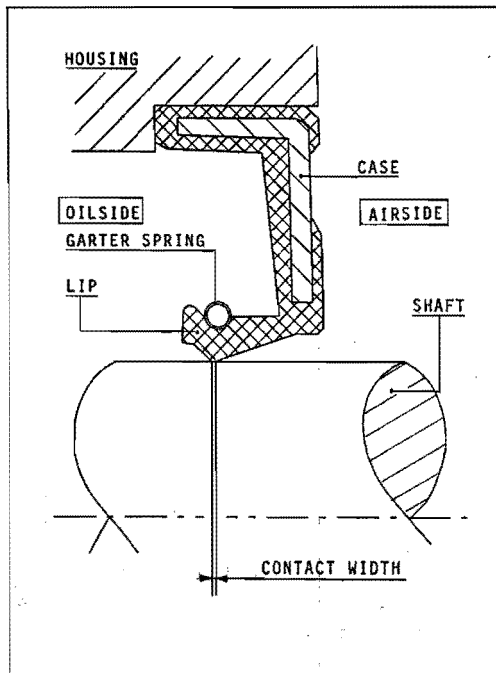


Fig. 1.1 : A standard radial lip seal.

Two important demands on radial lip seals are :

- 1) Minimal oil leakage.
- 2) Minimal friction losses.

These two demands contradict, e.g. an increase in contact force reduces leakage (temporarily) but increases friction losses and wear. It is the aim of the seal designer to find the optimal seal shape. Until now (1988) the designing of radial lip seals is a process mainly based on intuition, experience and trial-and-error.

1.2 OPTIMIZATION.

To come to a more optimal seal design :

- 1) a better qualitative understanding of the sealing and lubrication mechanism is necessary.
- 2) physical and mathematical models describing both mechanisms quantitatively are needed.

In the last 30 years intensive research has been done into radial lip seals. In the literature on radial lip seals a number of hypotheses and models have been presented to describe the sealing and lubrication mechanism.

1.3 STATE OF THE ART.

1.3.1 THE SEALING MECHANISM.

The models presented in literature to describe the sealing action of radial lip seals can be divided into passive and active models, figure 1.2.

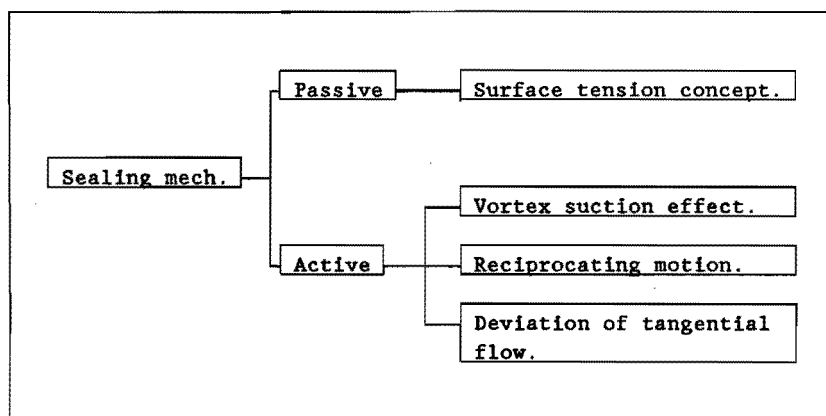


Fig 1.2 : Sealing concepts.

In 1957 Jagger [4] assumed that the surface tension of oil prevents the oil to leak through the sealing gap between seal and shaft. This passive sealing concept was further developed by Iny and Cameron (1966, [3]), Rajakovics (1971, [9]), and by Jagger and Wallace (1973, [10]). Later on, attention in seal research was focussed on the pumping action of seals. Kawahara and Hirabayashi (1977, [5]) described how seals start leaking when installed conversely, i.e. with the airside of the seal facing the bulk oil. Nowadays the pumping action of seals is often studied by injecting oil into the airside gap between seal and rotating shaft. A seal pumping rate is then defined by deviding the volume of injected oil by the time it takes the seal

to pump the oil to the oilside. The active models describing the pumping action can be divided into 3 concepts :

- 1) The vortex suction effect was described by Ott (1983, [8]). This suction effect is based on the formation of Taylor-Görtler vortices in the oil bulk, caused by shaft rotation.
- 2) Another concept is based on the presence of a reciprocating axial seal lip motion, relative to the shaft surface. This reciprocating motion can be caused by eccentricity of the seal or shaft. A reciprocating motion in combination with a non-symmetrical contact pressure distribution in the seal-shaft contact creates a net flow towards the side with the higher pressure gradient, i.e. the oilside of the seal, see Horve (1987, [2]).
- 3) Recently a lot of attention is paid to the concept of deviation of tangential flow. Here it is assumed that micro-asperities on the seal surface in the contact area cause a deviation of the tangential shear flow in axial direction, resulting in a net flow towards the oilside of the seal, see Müller (1987, [7]).

1.3.2 LUBRICATION MECHANISM.

Seal torque measurements indicate that the origin of friction of radial lip seals is hydrodynamic (or mixed) lubrication, see e.g. [13].

The basics of the 'parallel surface' lubrication mechanism of radial lip seals are not understood very well. The models presented in literature are based on a micro-elastohydrodynamic lubrication concept. Jagger and Walker [11] assume that deformed asperities on the seal contact area act as micro bearing pads. Hamilton, Walowit and Allen [12] have clarified that cavitation at the divergent side of micro-asperities can result in a positive load carrying capacity of the lubricating oil film. Hirano and Ishiwata [13] illustrate that the viscoelastic properties of the seal contact area can play an important role in the microasperity lubrication concept.

1.3.3 DISCUSSION.

A satisfactory verification of the sealing and lubrication concepts mentioned above is not described in literature. Most of the theoretical models described in literature are simple, qualitative models.

From literature research it can therefore be concluded that there is still little insight into the basic principles of the sealing and lubrication mechanism, and that there is no general consensus on the governing sealing mechanism.

1.4 OBJECTIVE OF THIS STUDY.

The objective of this study is to get a better insight into the sealing mechanism and the lubrication mechanism of radial lip seals.

1.5 COMPLICATIONS IN SEAL RESEARCH.

Investigating radial lip seals, one soon faces a number of problems :

1) A large number of parameters may influence the sealing and lubrication mechanism, such as physical properties of the oil, physical properties of the seal material, shaft diameter, shaft angular velocity, contact stress distribution, contact width, temperature, shaft roughness, out of roundness of the shaft, etc.

2) The seal-shaft contact is a highly non-linear (dynamic) contact problem, which can only be solved using advanced numerical tools. Further, the experimental determination and the mechanical characterisation of the nonlinear thermo-viscoelastic material behaviour of the rubber demands special attention.

3) Experimental determination of the physical quantities in the contact area such as local temperature $T(x)$, local contact pressure $p_0(x)$ or local film thickness $h(x)$, is difficult due to the small dimensions of the contact width b ($0.05 < b < 0.5\text{mm}$).

1.6 OUTLINE OF THIS THESIS.

The outline of this thesis can be summarized as follows :

- 1) General introduction (chapter 1)
- 2) Observations (chapter 2)
- 3) Contact conditions :
 - Static , Isothermal (chapter 3)
 - Static , Non-isothermal (chapter 4)
 - Contact temperature (chapter 5)
- 4) Sealing and lubrication models :
 - A pumping model (chapter 6)
 - A leakage model (chapter 7)
 - A VEHD lubrication model (chapter 8)
- 5) Conclusions (chapter 9)

In chapter 1 the reader is introduced to radial lip seals.

In chapter 2 the sealing mechanism is studied experimentally by under-lip observations.

In chapter 3 and 4, the isothermal respectively non-isothermal static seal-shaft contact problem is studied using nonlinear finite element analysis.

In chapter 5 methods to calculate and to measure the contact temperature are discussed.

In chapter 6 a model is presented describing the pumping action of the seal as observed in chapter 2.

In chapter 7 a model describing the leakage of seals at higher shaft angular velocities is presented.

In chapter 8 a visco-elastohydrodynamic (VEHD) lubrication model for seals is presented.

In chapter 9 final remarks are given, the main conclusions of this thesis are summarized and recommendations for future research are formulated.

1.7 GENERAL REMARKS.

1) On terminology :

In this thesis the word static refers to a situation where there is no radial motion of the shaft surface relative to the seal during shaft rotation. The word dynamic refers to a situation where there is a radial motion of the shaft surface during shaft rotation, e.g. due to out of roundness of the shaft.

2) On seal type :

All numerical and experimental data presented in this thesis are obtained for one specific commercially available Nitrile rubber radial lip seal with industrial code BAF 100x10x70, to be used on a nominal shaft diameter $d_1 = 70$ mm.

1.8 REFERENCES.

- [1] Deuring, H. Die Einfüsse auf die Function und die Gebrauchsdauer von Radial-Wellendichtungen. KEM (1967) 12. (In German)
- [2] Horve, L. A macroscopic view of the sealing phenomenon for radial lip seals. BHRA Intern. Conf. on Fluid Sealing 1987, Paper K2.
- [3] Iny, E.H., Cameron, A. The load carrying capacity of synthetic rubber rotary shaft seals. Proc. Instn. Mech. Engrs. Vol 181. 1966-1967.
- [4] Jagger, E.T. Rotary Shaft Seals: The sealing mechanism of synthetic rubber seals running at atmospheric pressure. Proc. Instn. mech. Engrs. 1957 vol 171, nr 18.
- [5] Kawahara, Y.; Hirabayashi, H. A study of sealing phenomena on oil seals. ASLE Transactions, Vol 22, 1977, pp 46-55.
- [6] Kammüller, M. Zur Abdichtwirkung von Radial-Wellendichtungen. Thesis Univ. of Stuttgart, Germany, August 18, 1986 (In German).
- [7] Müller, H.K. Concepts of sealing mechanism of rubber lip type rotary seals. Proc. BHRA 11th Int. Conf. on Fluid Sealing (1987) Paper K1.

- [8] Ott, G.W. Untersuchungen zum dynamischen Leckage und Reibverhalten von Radial-Wellendichtringen. Thesis Univ. Stuttgart, 10 Nov. 1983. (In German)
- [9] Rajakovics, G.E. Beitrag zur Kenntnis der Wirkungsweise von Berührungsdichtungen. Diss. TH-Wien, Germany, 1970. (In German)
- [10] Jagger, E.T., Wallace, D. Further experiments on the sealing mechanism of a synthetic rubber lip type seal operating on a rotating shaft. Instn. mech. Engrs. 1973 vol 187.
- [11] Jagger, E.T. ; Walker, P.S. Further studies of the lubrication of synthetic rubber rotary shaft seals. Proc. Inst. Mech. Engrs., Vol 181, no 9, 1966-1967, pp 101-204.
- [12] Hamilton, D.B.; Walowit, J.A.; Allen, C.M. Microasperity lubrication. Journal of basic Engineering, 1968, pp 351-355.
- [13] Hirano, F; Ishiwata, H. The lubrication condition of a lip seal. Proc. Instn. Mech. Engrs., Vol. 180, Pt. 3B, 1965-1966. Paper 15, pp 187-196.

CHAPTER 2 : THE SEALING MECHANISM, MEASUREMENTS AND OBSERVATIONS.

2.0 OVERVIEW.

2.1 Introduction.

2.2 The test-rig.

2.3 Observations using the glassfiber test-rig.

2.4 Discussion of the observations.

2.5 Drop in pressure over the oil-air interface.

2.6 Summary.

2.7 References.

Proper functioning radial lip seals exhibit a pumping action. They are able to pump oil from the airside to the oilside of the seal. In this chapter the pumping action is studied experimentally. From under-lip observations it is found that this pumping action is counterbalanced by capillary suction forces of the oil-air interface on the airside of the seal. Cavitation was observed on the edges of the contact area.

2.1 INTRODUCTION.

Radial lip seals are able to pump oil from the airside of the seal to the oilside. This pumping action has been studied by other investigators by injecting oil into the airside gap between the seal lip and the rotating shaft surface, [1,4]. A seal pumping rate is then defined by deviding the amount of injected oil by the time it takes the seal to pump the oil to the oilside.

Here this oil-injection method is not used, because the injection of oil leads to transient operating conditions, as will be explained below. In this chapter under-lip observations of the pumping action are discussed. Using the results of these observations an attempt is made to calculate the seal pumping pressure under steady-state operating conditions.

2.2 THE TEST-RIG.

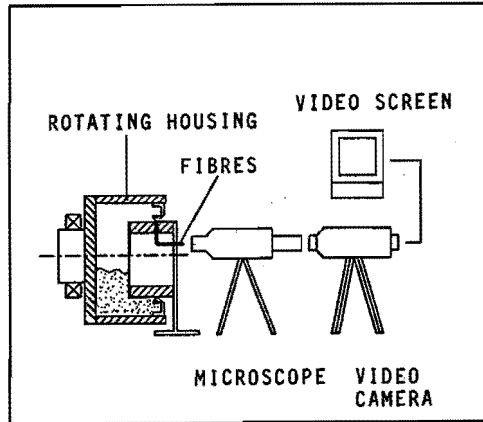


Fig. 2.1 : Glassfibre test-rig to study the under-lip contact area.

Using the test-rig as represented in figure 2.1 the under-lip contact area was studied. The test-rig consists of a seal rotating on a fixed hollow steel shaft. A square bundle (1.7 mm x 1.7 mm) of 50,176 square step-index multi-mode glassfibres of each $2.5 \mu\text{m} \times 2.5 \mu\text{m}$, was adjusted into the steel hollow shaft. Via the glassfibres under-lip video registrations were made through a microscope. Compared to the test-rig as used by other investigators who studied the contact area through a rotating transparent thin hollow perspex shaft via a mirror and microscope, the test-rig of figure 2.1 has some important advantages :

- 1) The contact conditions such as shaft roughness and wetting angle oil-steel are only changed in a small region of 0.7 % of the circumference of the shaft, where the seal is not running on the shaft surface but on the end of the glassfibre bundle which was given the same radius as the shaft surface.
- 2) The thermal boundary conditions, i.c. the heat transfer properties of the shaft are hardly influenced by the small glassfibre bundle. Compared to a hollow shaft of steel, a hollow shaft of perspex has not only inferior heat transfer properties due to a lower thermal conductivity ($\lambda_{\text{steel}} / \lambda_{\text{perspex}} = 52 / 0.19 = 274$), but also due to the fact that the hollow perspex shaft has to be very thin to prevent optical distortion.

A disadvantage of the glassfiber test-rig is that the seal rotates and the shaft is fixed, whereas in most seal applications in practice the shaft rotates and the seal is fixed. To study the influence of centrifugal forces on the contact conditions in case of a rotating seal, FEM calculations were performed taking into account these centrifugal forces, see chapter 3.6.

2.3 OBSERVATIONS USING THE GLASSFIBER TEST-RIG.

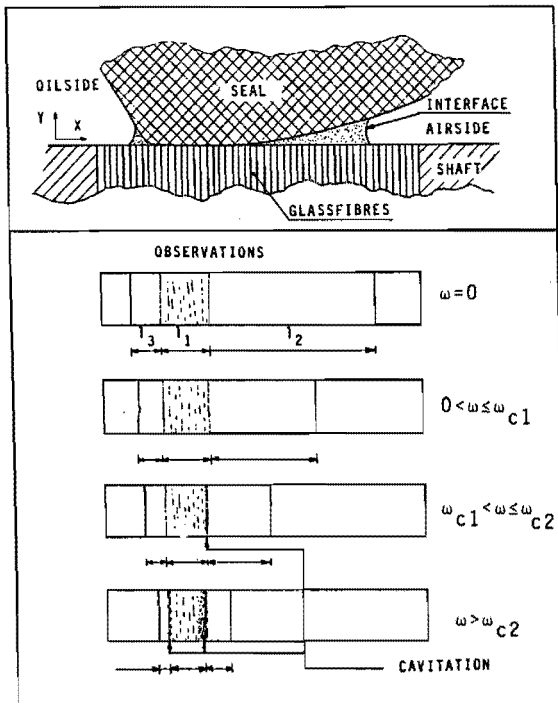


Fig. 2.2 : Schematic drawing of the contact area.

On basis of figure 2.2 the experimental observations performed with the glassfibre test-rig are summarized as follows :

- 1) Starting at seal angular velocity $\omega_2 = 0$, a gradual increase in ω_2 resulted in a simultaneously decrease of l_1 , l_2 and l_3 . Reducing ω_2 to $\omega_2 = 0$ again, l_1 , l_2 and l_3 increased to their starting values.
- 2) For a certain set of operating conditions (ω_2, η, T) a steady-state situation occurred, where l_1 , l_2 and l_3 remained constant.

- 3) For $\omega_2 > \omega_{c1}$ cavitation occurred in a small region on the airside of the contact area as illustrated in figure 2.2. For $\omega_2 > \omega_{c2}$ a second cavitation region occurred on the oilside. The intensity of the cavitation and the width of the cavitation regions increased as ω_2 increased further. In our case was $\omega_{c1} \approx 60$ [rad/s] and $\omega_{c2} \approx 95$ [rad/s].
- 4) The oil-air interface on the oilside was instable and oscillated in axial direction during shaft rotation, whereas the oil-air interface on the airside was stable, and did not oscillate.

During the experiments no detectable leakage from the oil- to the airside of the seal was found. There was no pressure difference between the oil- and the airside of the seal.

2.4 DISCUSSION OF THE OBSERVATIONS.

- 1) The decrease in l_2 , when increasing ω_2 , can be explained by active pumping of the seal. The seal pumps the oil from the airside to the oilside. A decrease of l_2 results in an increase of the capillary suction forces. As l_2 decreases, the gap height $h(x)$ between shaft- and seal surface becomes smaller and the radius of the oil-air interface will decrease, resulting in an increased pressure drop over the oil-air interface, or in other words, an increase of the capillary suction forces.
- 2) In the steady-state situation the pumping action of the seal is counterbalanced by the capillary suction forces. These capillary forces are determined by the wetting angles, the surface tension and the gap height.
- 3) Cavitation can be caused by pressure drops in the valleys of microasperities on seal or shaft surface, see [6]. Cavitation occurs on both edges of the contact area because here the average oil pressure is lower than in the middle of the contact area. The occurrence of cavitation also depends on local temperatures and on the local shape of the micro-roughness of the surfaces.
- 4) On those locations where the bulk oil is not directly in contact with the seal, an (instable) oil-air interface can be formed on the oilside of the seal also.

The observations indicate that an active pumping action is responsible

for the sealing mechanism, not the surface tension of the oil-air interface as assumed by Jagger [2] and Rajakovics [3]. The capillary suction forces play an important role in the lubrication mechanism; without the counteracting pumping action of the capillary forces the oil in the contact area would be pumped to the oilside of the seal resulting in starved lubrication. Colouring the oil with ink, Nijssen [7] found that, also in steady-state situations, there is a mutual exchange of oil between the oilside and airside of the seal. However, there is no net flow of oil in axial direction in steady-state situations.

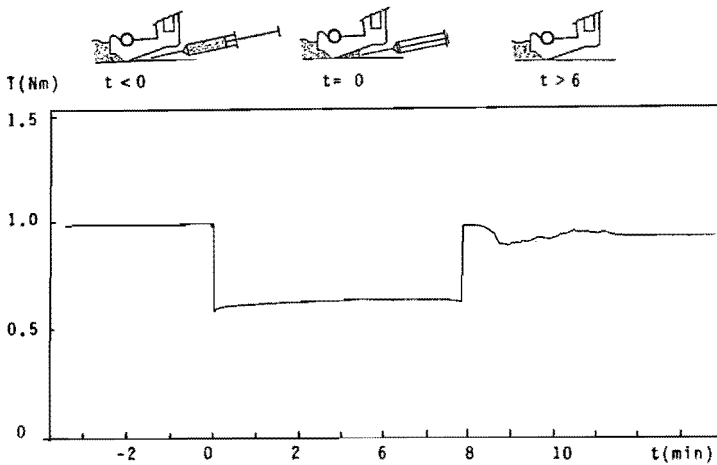


Fig. 2.3 : Instationary torque signal during pumping action. Shaft angular velocity $\omega_1 = 105,6$ rad/s (16.8 Hz). Volume of injected oil (Shell Tellus 46) $v_{oil} = 500$ mm³

In the more recent literature on radial lip seals it is often assumed that a good seal is a seal which has a high pumping rate. This assumption should be considered with care. A good seal is a seal with a high sealing performance, and a long service life. A very high pumping rate may lead to starved lubrication, resulting in wear of the seal contact area and premature failure. Further care should be taken when studying the pumping effect experimentally by injecting oil in the gap between seal and shaft on the airside of the seal. Then a transient situation is created which does not correspond to the normal steady-state running conditions. Directly after injection, the pressure drop over the oil-air interface is reduced due to a sudden increase in l_2 . The influence of this effect on the pumping action is not clear yet, but its influence on the lubrication condition can be

concluded from the considerable decrease in torque, measured during the pumping action, see fig. 2.3. Therefore an attempt is made to determine the pumping action for a steady-state situation by calculating the pressure drop over the oil-air interface.

2.5 DROP IN PRESSURE OVER THE OIL-AIR INTERFACE.

On the airside there is a drop in pressure over the oil-air interface. This pressure drop can be written as:

$$\Delta p = \frac{\gamma}{R} \quad (2.1)$$

where γ is the surface tension of the oil and R is the radius of the oil-air interface. In our case R is determined by the distance x , the gap height $h(x)$ and the wetting angles α_1 for oil-steel and α_2 for oil-rubber, thus $R = R(x, h(x), \alpha_1, \alpha_2)$. R can be calculated by solving equation (A1.8), see appendix A1.

Figure 2.4 gives the calculated pressure drop over the oil-air interface as function of l_2 . The function $h(x)$ was determined from the deformed seal contour, calculated with the FEM, see chapter 3. In order to study the pumping action of the seal, $l_2 = l_2(\omega_2)$ was determined experimentally using the glassfiber test-rig, see figure 2.5. With these measured data and equation (2.1) the pumping pressure $\Delta p = \Delta p(\omega_2)$ was calculated, see figure 2.6

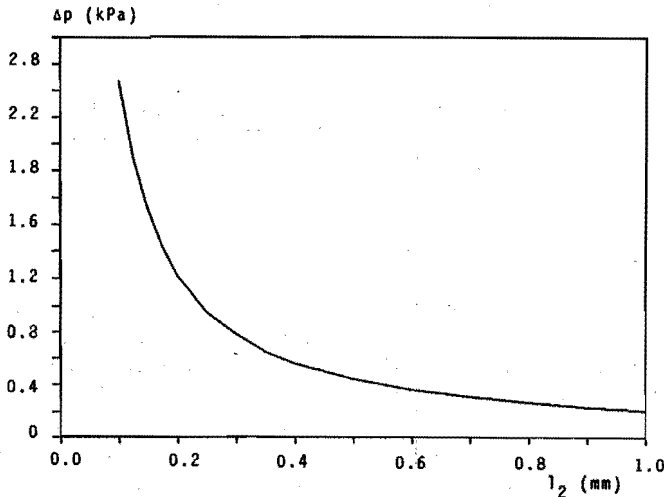


Fig. 2.4 Calculated pressure drop over oil-air interface as function of the distance between the oil-air interface on the airside and the contact area, $\Delta p = \Delta p(l_2)$.

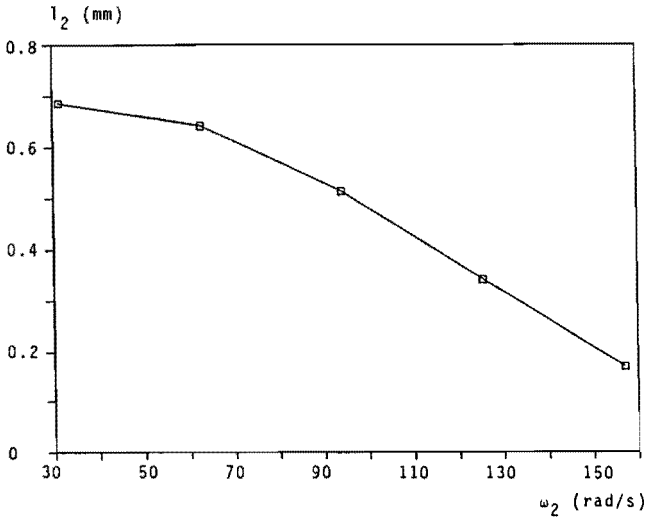


Fig. 2.5 : The distance from the oil-air interface on the airside to the contact area as function of the seal angular velocity, $l_2=l_2(\omega_2)$, measured using the glassfibre test-rig.

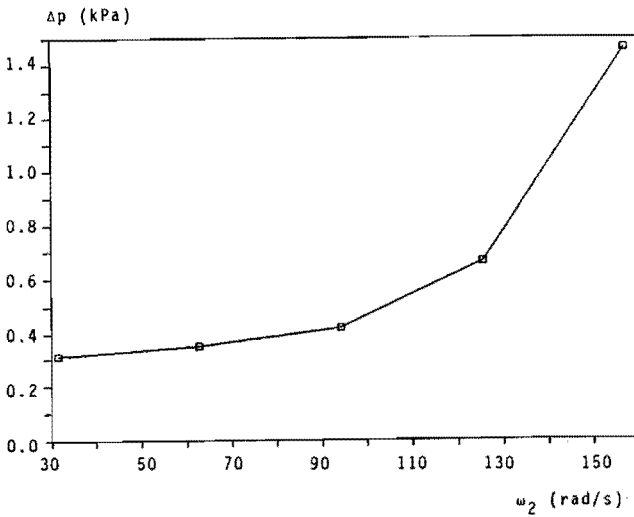


Fig. 2.6 : Calculated pressure drop over oil-air interface as function of the seal angular velocity, $\Delta p= \Delta p(\omega_2)$, calculated with the measured data $l_2=l_2(\omega_2)$.

2.6 SUMMARY.

- 1) The sealing mechanism of radial lip seals is based on an active pumping action.
- 2) In a steady-state situation the pumping action of the seal is counterbalanced by the capillary suction forces of the oil-air interface on the airside.
- 3) Without the counteracting action of the capillary forces, the seal pumping action would cause starved lubrication.
- 4) Cavitation occurs first on the outer edges of the contact area.

In order to come to a better understanding of the sealing mechanism there is a strong need for a physical model, which describes the active pumping mechanism. A first step towards such a model is described in chapter 6. The seal-shaft contact conditions such as the contact stress distribution and the contact temperature form the boundary conditions for the pumping model. These contact conditions will be studied in chapters 3,4 and 5.

2.7 REFERENCES.

- [1] Kammüller, M. Zur Abdichtwirkung von Radial-Wellendichtringen. Thesis 1986, Univ. of Stuttgart, Germany. (In German)
- [2] Jagger, E.T. Rotary Shaft Seals: The sealing mechanism of synthetic rubber seals running at atmospheric pressure. Proc. Instn. mech. Engrs. 1957 vol 171, nr 18.
- [3] Rajakovics, G. Beitrag zur kenntnis der Wirkungsweise von Berührungsdichtungen. Diss. Wein,1970. (In German)
- [4] Müller, H.K. Concepts of sealing mechanism of rubber lip type rotary shaft seals. Proc. 11th Conf. on Fluid Sealing. BHRA, 1987, paper K1, pp 698-709.
- [5] Adam, N.K. The Physics and chemistry of surfaces. Dover Publications Inc. N.Y.,1968.
- [6] Hamilton, D.B.; Walowit, J.A.; Allen, C.M. Microasperity lubrication. Journal of Basic Engineering, 1968, pp 351-355.
- [7] Nijssen, G.F. Het afdichtmechanisme by Simmerringen. M.Sc.Thesis, Eindhoven University of Technology, Sept. 1986.(In Dutch)

CHAPTER 3 : THE SEAL-SHAFT CONTACT: STATIC, ISOTHERMAL CONDITIONS.

3.0 OVERVIEW

- 3.1 Introduction.
- 3.2 Material characterisation.
- 3.3 FEM model definition.
- 3.4 Discussion of the FEM results.
- 3.5 Rubber swelling.
- 3.6 Centrifugal forces.
- 3.7 Summary.
- 3.8 References.

Studying the sealing mechanism it is important to know the contact stress distribution p_0 in the contact area. In the present chapter the static, isothermal seal-shaft contact problem is studied by a nonlinear finite element analysis.

3.1 INTRODUCTION.

The seal-shaft contact problem is nonlinear because of 3 effects

- 1) Geometrical nonlinearity
- 2) Physical nonlinearity
- 3) Nonlinear boundary conditions.

The problem is geometrically nonlinear due to the large deformations which occur in the deformed seal lip. The problem is physically nonlinear because the rubber material behaviour is nonlinear, thus Hooke's law does not apply. Finally the problem is nonlinear because of the nonlinear boundary conditions in the contact area, which vary as function of the contact stress.

Due to these nonlinearities the seal-shaft contact problem is too complex to be solved analytically. The contact problem was therefore studied numerically using the finite element method (FEM). The FEM is a numerical discretization technique very useful for stress/strain analysis and heat analysis of mechanical structures, see e.g. [1].

3.2 MATERIAL CHARACTERISATION.

An important complication in the use of the FEM for stress/strain analysis of deformed seals is the appropriate characterization of the mechanical behaviour of the synthetic rubber seal material. The reliability of the numerical output of FEM calculations depends on the accuracy of the constitutive law which describes the mechanical material behaviour. The parameters of these constitutive laws vary for each synthetic rubber and have to be determined experimentally. Synthetic rubbers exhibit a material behaviour, which is rather complex compared with the material behaviour of materials like steel. Rubbers exhibit an (almost) incompressible, nonlinear thermo-viscoelastic material behaviour. Incompressible indicates that there will be no volume change under a hydrostatic pressure, thus that the Poisson ratio $\nu = 0.5$. Nonlinear refers to the relationship between stresses and strains; the stiffness of rubber is not constant, but a function of the strain. Thermo-viscoelastic means that the mechanical material behaviour is not only a function of temperature, but that also viscous- or time effects, such as creep and stress relaxation occur.

With respect to the viscoelastic material behaviour of rubber it is important to make a distinction between the stiffness of rubber under static load and the stiffness of rubber under dynamic load. Chapters 3,4,6 and 7 are restricted to static conditions, here the influence of the parameter time is not taken into account. The question arises if it is allowed to assume static conditions in case of a rotating shaft. Out of roundness, eccentricity or vibrations of the shaft will result in a (small-amplitude) dynamic excitation of the seal lip. The influence of this dynamic load on the seal stiffness and thus on the contact conditions is difficult to model. Attempts to study these dynamic effects will be discussed in chapter 8.

3.3 FEM MODEL DEFINITION.

To determine the undeformed seal geometry for the FEM model, a cross-section was made of a virgin undeformed seal imbedded in transparent resin. The seal-shaft contact problem was modeled using the nonlinear FEM program ABAQUS, [3]. The problem was assumed to be axisymmetric and isothermal. Non-isothermal situations will be discussed in chapter 4. Assuming that only the flexible part of the seal below the metallic case will deform, only this part was modeled, see fig. 3.1. The FEM model consists of 355 4-node, bi-linear displacement, constant pressure axisymmetric ring elements. These hybrid elements are especially intended for use with incompressible material behaviour. To

describe the seal-shaft contact, 2-node interface elements have been used. On one end these interface elements interact with the seal, on the other end with a rigid (shaft) surface. No friction was assumed in the contact. The garter spring was modeled using 6 multiple point constraints and 1 linear spring element. The multiple point constraints restrain the displacements but not the rotations and provide a pinned rigid link between nodes on the lip and the node at the end of the spring element k_s .

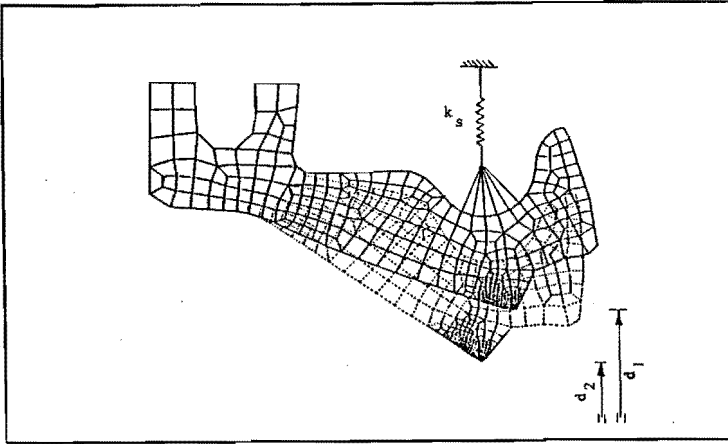


Fig. 3.1 Finite element mesh used for calculations on a radial lip seal in undeformed and deformed condition.

Simple numerical tests were performed to provide an elementary verification of the element model. The hybrid elements in combination with a Mooney-Rivlin material model have been used to calculate the uniform radial deformation of a rubber cylinder, under plane strain conditions, subjected to an internal pressure. The numerical results showed good correspondence with the exact solution from [6]. The interface elements were tested on a simple linear Hertz contact problem. Again a good correspondence between the numerical and the analytical solution was found. Finally the element model of the garter spring was verified by a simple analytical model.

In the FEM model the mechanical behaviour of the rubber material was assumed to be homogeneous and isotropic. The mechanical behaviour of the rubber material was approximated using the hyperelastic Mooney-Rivlin model [7]. This model is based on the assumption that (a) the material is incompressible and isotropic, and (b) that Hooke's law is obeyed in simple shear.

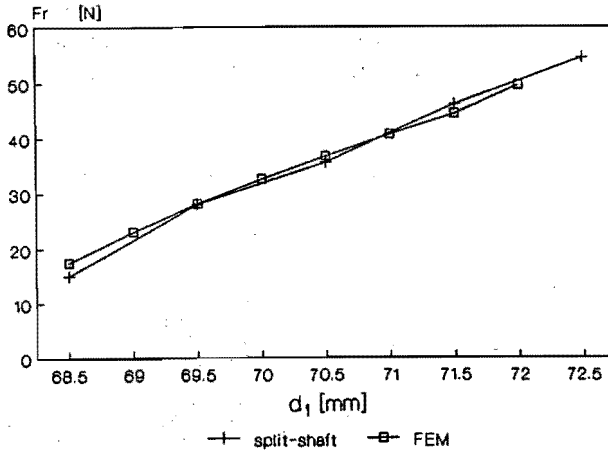


Fig. 3.2 : Contact force $F_r = F_r(d_1)$ after $t=24$ hours at temperature $T= 30$ °C, calculated with the finite element method (FEM) and measured with a split-shaft device, for a radial lip seal of Nitrile rubber, including a garter spring. Nominal shaft diameter $d_1= 70$ mm.

On basis of these assumptions Mooney has derived for the strain energy function W :

$$W = C_1(\lambda_1^2 + \lambda_2^2 + \lambda_3^2 - 3) + C_2(\lambda_1^{-2} + \lambda_2^{-2} + \lambda_3^{-2} - 3) \quad (3.1)$$

where $\lambda_i = \frac{l_i + \Delta l_i}{l_i}$ is the stretch ratio in main direction i .

The theoretical form of the stress-strain curve for simple uni-axial extension can be derived to be :

$$\sigma = 2(\lambda_1 - \lambda_1^{-2}) \cdot (C_1 + C_2/\lambda_1) \quad (A5.2)$$

The 2 constants $C_1 = -2.746$ and $C_2 = 4.597$ MPa have been obtained from curve-fits on experimental data from isothermal uni-axial stress-relaxation tests on Nitrile rubber specimen after a relaxation time of $t=24$ hours at $T=30$.°C, at different stretch ratios λ_1 , see ten Hagen [4].

3.4 DISCUSSION OF THE FEM RESULTS.

Figure 3.2 shows the measured and calculated values of the radial contact force F_r for a Nitrile rubber lip seal for different shaft diameters at a constant temperature $T = 30^\circ\text{C}$ after $t = 24$ hours. The contact force was measured on a split-shaft measuring device, see Luyten [5]. Considering the complexity of the problem (physically nonlinear, geometrically nonlinear and nonlinear boundary conditions) the correspondence between the measured and calculated results is remarkable.

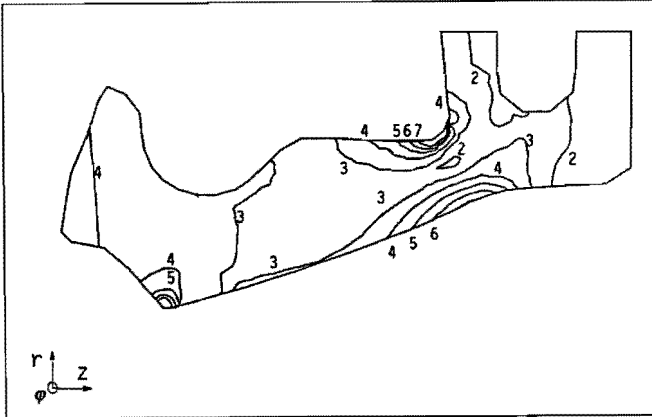


Fig. 3.3 : Von Mises stress σ_{vm} distribution in the seal. Contact width $b = 0.075$ mm. Stress levels :
1= 0.0 2= 0.1 3= 0.2 4= 0.3 5= 0.4 6= 0.5 7= 0.6 MPa

Figure 3.3 shows a plot of the von Mises stresses σ_{vm} in the lip of the seal. Two relative maxima of σ_{vm} occur at the hinge point of the seal lip on the airside and on the oilside. The absolute maximum $\sigma_{vm} = 3.69$ MPa occurs in the lip at approximately 0.01 mm above the seal-shaft contact close to the oilside of the seal, see fig. 3.4. The maximum of the principal stresses in radial direction $\sigma_{rr} = -4.73$ MPa occurs also close to the oilside, but directly in the contact area, see fig 3.5. It is well-known in literature that for proper functioning seals it is necessary that the maximum of the static contact pressure distribution p_0 occurs on the oilside of the contact, see also chapter 6.

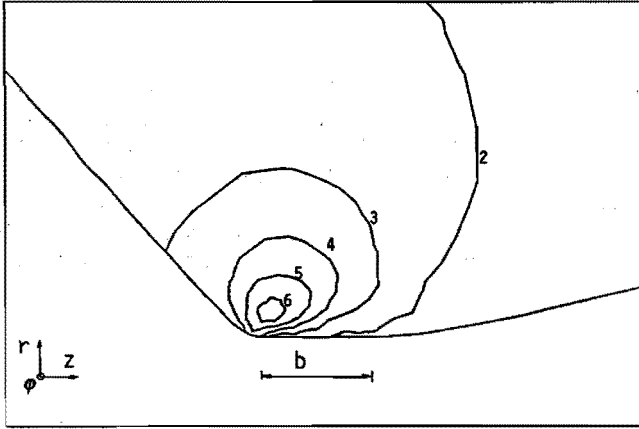


Fig. 3.4 : Von Mises stress σ_{vm} distribution in tip of the lip.
Stress levels :
1= 0.0 2= 0.5 3= 1.0 4= 1.5 5= 2.0 6= 2.5 MPa.

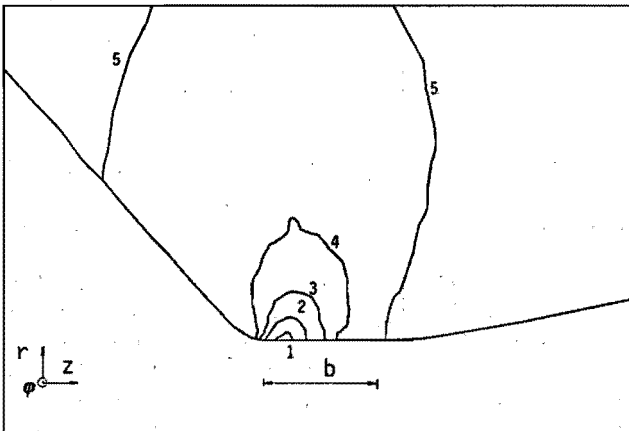


Fig. 3.5 : Principal radial stress σ_{rr} distribution in tip of the lip. Stress levels :
1= -4.5 2= -3.5 3= -2.5 4= -1.5 5= -0.5 6= +0.5 MPa.

3.5 RUBBER SWELLING.

Though a detailed discussion of the influence of swell is not within the scope of this study, it is worthwhile to mention briefly rubber swelling here, because it is usually neglected. When rubber is immersed in oil, the oil migrates into the rubber because of inter-molecular attraction. Simultaneously, plasticisers, anti-oxidants, and accelerator decomposition products can be extracted from within the rubber. If the rate of migration of oil into the rubber is greater than the rate of extraction of materials, the rubber will swell. Conversely, shrinkage can occur. The degree of volume change is influenced by temperature and the chemical nature of the oil. Swell results in a decreased interference between the seal lip and shaft, whereas shrinkage results in an increased interference. Swell and shrinkage also influence the rubber stiffness, see [2].

3.6 CENTRIFUGAL FORCES.

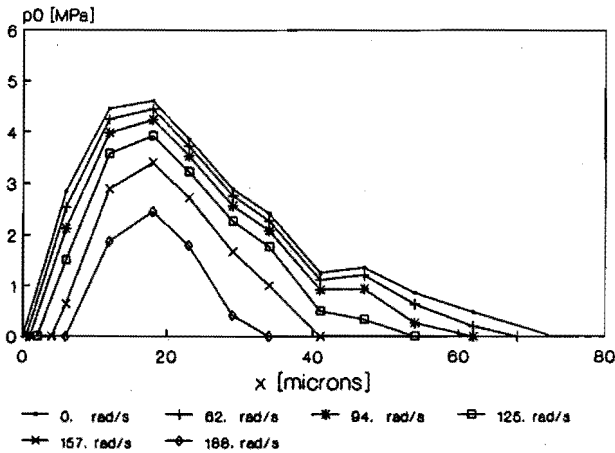


Fig. 3.6 : Contact stress distribution p_0 under the influence of centrifugal forces as function of the seal angular velocity ω_2 , calculated with the FEM for $d_1 = 70$ mm ; $T = 30$ °C ; $t = 24$ h ; $\rho_{\text{seal}} (\text{Nitrile}) = 1.46 \cdot 10^3$ kg.m⁻³ ; $m_{\text{spr}} = 2.75 \cdot 10^{-3}$ kg.

In most practical situations the shaft rotates whereas the seal is fixed. In some seal applications and also in the test-rig described in chapter 2, the seal is rotating on a fixed shaft. To study the

influence of centrifugal forces on the contact conditions FEM calculations have been performed taking into account these centrifugal forces. Figure 3.6 shows the influence of centrifugal forces on the static contact pressure distribution p_0 . Note that not only p_0 decreases but that also the non-symmetrical profile of p_0 becomes more symmetric as the seal angular velocity ω_2 increases. This decrease in p_0 and particularly the more symmetric distribution of p_0 could be responsible for the fact that rotating seals start leaking at lower angular velocities than fixed seals on rotating shafts, see also chapter 8.

3.7 SUMMARY

- 1) The static contact force calculated with a nonlinear FEM model using a Mooney-Rivlin material model showed good correspondence with the measured contact force.
- 2) The static contact stress distribution is nonsymmetric, and has a maximum located on the oilside of the contact area.
- 3) Centrifugal forces acting on a rotating seal do not only reduce the contact stress and contact width, but also result in a more symmetric contact stress distribution.

The results presented in this chapter are all calculated for an isothermal situation at $T=30$ °C. In practical situations a (transient or steady-state) non-isothermal situation will occur due to a raise in contact temperature in consequence of the dissipated friction heat. Steady-state non-isothermal situations are discussed in the next chapter.

3.8 REFERENCES.

- [1] Bathe, KJ. Finite Element Procedures in Engineering Analysis. Prentice-Hall Inc., Englewood Cliffs, New Jersey 07632, 1983.
- [2] Taylor, K.R.; Griffiths, A. Some factors of rotary shaft seal design and effects of lubricants on related elastomers. Tribology International, December 1977, pp 306-313.
- [3] Hibbit, Karlson and Sorensen ABAQUS FEM software, user manuals (version 4-5).

- [4] Hagen ten, E.A.M. Mechanische karakterisering van afdichtingsrubbers . M.Sc. Thesis, Eindhoven Univ. of technology, Jan. 1988. (In Dutch)
- [5] Luyten, R. Bepaling van de radiaalkracht, contactbreedte en contactspanningsverdeling bij simmerringen . M.Sc. Thesis, Eindhoven Univ. of Techn., Dec 1987. (In Dutch)
- [6] Green, A.E. ; Zerna, W. Theoretical Elasticity., Oxford University Press, London, 1986.
- [7] Treolar, L.R.G. The physics of rubber elasticity. Clarendon Press, Oxford, 1975.

CHAPTER 4 : THE SEAL-SHAFT CONTACT: STATIC, NON-ISOTHERMAL CONDITIONS.

4.0 OVERVIEW.

- 4.1 Introduction.
- 4.2 Temperature effects.
- 4.3 Temperature distribution in the seal.
- 4.4 Influence of temperature on the contact conditions.
- 4.5 Discussion of the results.
- 4.6 Summary.
- 4.7 References.

The influence of temperature on the static seal-shaft contact problem is studied using a coupled stress-temperature FEM analysis.

4.1 INTRODUCTION.

In chapter 3 the contact conditions for an isothermal situation were discussed. In practice non-isothermal situations will occur, because the friction heat generated in the seal-shaft interface results in a raise in seal lip temperature.

Investigating the sealing mechanism of radial lip seals it is important to know the influence of temperature on the contact conditions such as contact force, contact width and contact stress distribution, because they are the boundary conditions for the sealing and lubrication mechanism.

4.2 TEMPERATURE EFFECTS.

A distinction can be made between (a) irrerversible and (b) rerversible temperature effects on the contact conditions. Some examples of irrerversible temperature effects are :

- 1) Influence of temperature on physical ageing, resulting in a permanent change in stiffness of the rubber.
- 2) Influence of temperature on chemical ageing due to chemical reactions between oil(-additives) and rubber.
- 3) Influence of temperature on swell of the rubber due to absorbtion of oil(-additives).

The irreversible temperature effects will not be discussed in detail. In this chapter we will confine ourselves to the following reversible temperature effects.

- 1) Influence of temperature on the stiffness of the rubber.
- 2) Influence of the temperature on the stiffness and initial length of the garter spring.
- 3) Thermal expansion of the seal material.
- 4) Thermal expansion of the shaft.

To study the influence of these reversible temperature effects on the contact conditions, information is needed on the temperature distribution in the seal.

In principle the temperature distribution in the seal can be determined in a number of different ways, e.g. by analytical models [1], by the finite difference method [2], by the boundary element method [3], or by the finite element method [4]. In this chapter the finite element method was chosen because using this method, a coupled stress-temperature analysis is possible.

4.3 TEMPERATURE DISTRIBUTION IN THE SEAL.

In chapter 3 it was shown that isothermal FEM calculations of the contact force of a Nitrile rubber lip seal using the Mooney-Rivlin material model showed very good correspondence with experimental contact force measurements. A coupled stress-temperature FEM analysis was performed, assuming that the stress is dependent on the temperature distribution, but that there is no inverse dependence. The thermal stresses had only a very minor influence on the deformed shape of the seal. Therefore it was assumed that the temperature distribution was not dependent on the stresses. The temperature distribution was calculated using the deformed seal geometry from chapter 3. The calculated temperature field was then used as an input for the coupled stress-temperature analysis. In the coupled analysis the 2 Mooney-Rivlin constants depend on temperature. In this paragraph the temperature distribution is discussed. In the next paragraph the influence of the temperature distribution on the contact conditions is investigated.

The heat problem was assumed to be axisymmetric and the ABAQUS FEM model [7] contained 676 4-node, linear, axisymmetric ring, heat transfer elements. The garter spring and the metallic case were given the thermophysical properties of steel. It was assumed that the thermophysical material properties and the convective boundary conditions are not temperature dependent, thus the heat analysis

problem was assumed to be linear. Note however, the stress/strain analysis of the contact problem remains nonlinear. See table 4.1 for the (thermo-) physical properties of Nitrile rubber and steel. The following thermal boundary conditions were prescribed on boundaries Γ_1 , Γ_2 , Γ_3 and Γ_4 (see fig 4.1) :

- 1) Γ_1 : Fixed temperature T_m where the seal is in contact with the machine housing.
- 2) Γ_2 : Fixed temperature T_c in the seal-shaft contact area.
- 3) Γ_3 : Convection to oil on oilside of the seal, for oil bulk temperature T_{oil} and film coefficient h_{oil} .
- 4) Γ_4 : Convection to air on airside of the seal, for air temperature T_{air} and film coefficient h_{air} .

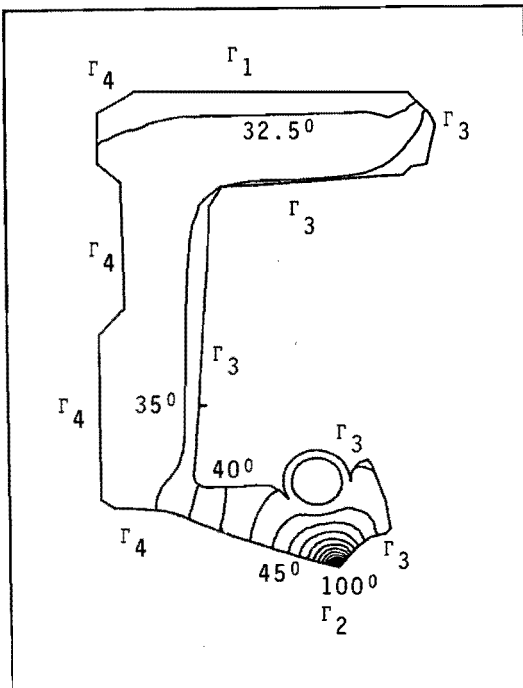


Fig. 4.1 : Steady-state temperature distribution in the radial lip seal of Nitrile rubber, calculated with the finite element method, for case 5 of table 4.2.

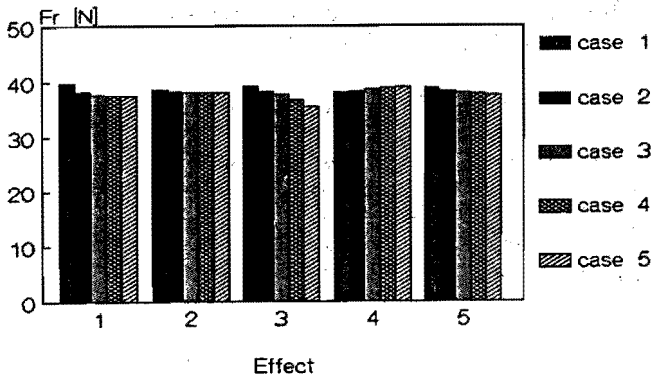


Fig. 4.2 : The contact force F_r for the 5 different cases of table 4.2 and for 5 effects, calculated by a coupled stress-temperature FEM analysis. The effects are :

- 1 Influence of temperature on material stiffness.
- 2 Influence of temperature on spring stiffness.
- 3 Influence of thermal expansion of the rubber.
- 4 Influence of thermal expansion of the steel shaft.
- 5 Combined effect of 1), 2), 3) and 4).

The steady-state temperature distribution in the seal was calculated for 5 different sets of boundary conditions as represented in table 4.2. Figure 4.1 shows the steady-state temperature distribution in a seal calculated with the FEM model for case 5 of table 4.2. With case 2 as initial condition the steady-state temperature distribution was reached after a transient time of 25 minutes.

The values of film coefficients h_{air} and h_{oil} are estimates based on formulae given in [5].

		Nitrile	Steel
Specific mass	ρ [kg.m ⁻³]	1460.	7800.
Thermal conductivity	λ [W/mK]	.43	50.
Specific heat	c [J/kgK]	2000.	450.
Thermal expansion coeff.	α [1/K]	$9.44 \cdot 10^{-5}$	$1.1 \cdot 10^{-5}$

Table 4.1 : Thermo-physical properties of Nitrile rubber and steel.

case	T_c [°C]	T_{air} [°C]	T_{oil} [°C]	T_m [°C]	h_{air} [W/m ² K]	h_{oil} [W/m ² K]
1	0.	0.	0.	0.	0.	0.
2	20.	20.	20.	20.	0.	0.
3	50.	20.	30.	20.	10.	200.
4	75.	20.	35.	20.	10.	200.
5	100.	20.	40.	30.	10.	200.

Table 4.2 : Thermal boundary conditions for 5 cases.

4.4 INFLUENCE OF TEMPERATURE ON THE CONTACT CONDITIONS.

The influence of the 4 reversible temperature effects on the contact force for the 5 cases of table 4.2 is summarized in figure 4.2. Case 2 was chosen as the starting or reference situation.

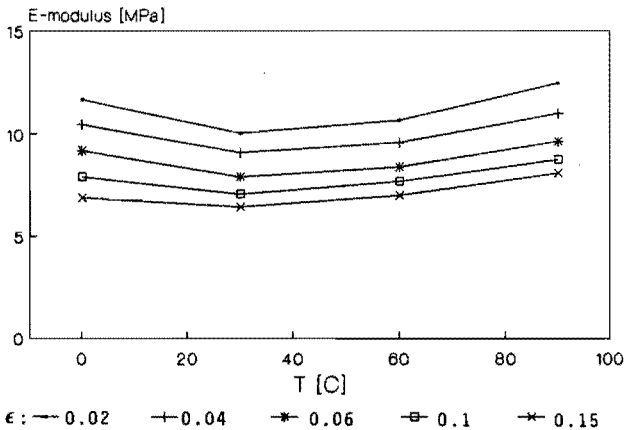


Fig. 4.3 : E-modulus of Nitrile rubber as function of temperature for different strains $\epsilon = \Delta l/l$ after a relaxation time $t=24$ h.

Figure 4.3 shows the E-modulus determined from (quasi-)static isothermal uni-axial stress-relaxation tests on Nitrile rubber specimen. Using these experimental data the Mooney constants C_1 and C_2 were determined as function of the temperature. The (reversible) influence of the temperature on the seal material stiffness results in a change in contact force as represented in column 1 of figure 4.2. The

stiffness of the garter spring and its initial length are both a function of temperature. The influence of this temperature effect on the contact force is shown in column 2. The influence of thermal expansion of Nitrile rubber on the contact force is shown in column 3. Column 4 shows the influence of thermal expansion of the shaft on the contact force. Column 5 shows the influence of the 4 effects together. With 10 nodes (9 elements) in the contact width ($b=0.075$ mm) no change in contact width was found for all 5 cases, and only very minor changes in contact stress distribution occurred.

4.5 DISCUSSION OF THE RESULTS.

The influence of the temperature on the contact conditions is relatively small for the 5 cases described above. However, it is worthwhile to consider that :

- 1) It is the aim of the seal manufacturer to produce a seal that is not very sensitive to changes in temperature. Thus a rubber is chosen which stiffness is not very temperature dependent. Also the garter spring has received a special temperature treatment to reduce the influence of temperature on the spring stiffness.
- 2) Only a relatively small zone in the tip of the seal is exposed to higher temperatures, see figure 4.1.
- 3) In practice often contact temperatures higher than $T_c=100$ °C of case 5 will occur. These higher temperatures were not taken into account in the FEM analysis. For temperatures above 100 °C the rubber stiffness rapidly changed due to physical ageing (additional vulcanisation), resulting in an irreversible change of rubber stiffness.
- 4) Although the influence of temperature on the static stiffness of Nitrile rubber is relatively small (see fig. 4.3), temperature can have a strong influence on the rubber stiffness under a dynamic load. The dynamic stiffness becomes important in case of dynamic excitation of the seal lip due to eccentric movements of the shaft center or due to out of roundness of the shaft, see chapter 8.

4.5 SUMMARY.

For the Nitrile rubber lip seal under investigation, the influence of the contact temperature T_c on the static contact conditions is neglectably small for $0 < T_c < 100$ °C.

As a result the static isothermal contact conditions as determined in chapter 3 will be used in the following chapters.

4.6 REFERENCES.

- [1] Upper, G. Dichtlippentemperatur von Radial-Wellen Dichtungen. Thesis University of technology of Karlsruhe, Germany ,21 July 1967. (In German)
- [2] Ozisik, M.N. Heat Transfer, a basic approach. Mc Graw-Hill Book Company, New York 1985.
- [3] Brebbia, C.A. Applications of the boundary element method for heat transfer problems. Rev. Gen. Therm. Fr. no 280, April 1985.
- [4] Bathe, KJ. Finite Element Procedures in Engineering Analysis. Prentice-Hall, Inc., Englewood Cliffs, New Jersey 07632, 1982.
- [5] Wong, H.Y. Handbook of essential formulae and data on heat transfer for engineers, Longman, London and New York, 1977.
- [6] Luyten, R. Bepaling van radiaalkracht, contactbreedte, en contactspanningsverdeling bij Simmerringen (in Dutch). M.Sc. Thesis, Eindhoven Univ. of Techn., Dec 1987.
- [7] Hibbit, Karlson and Sorensen
ABAQUS FEM software, user manuals (version 4-5)
- [8] MARC Analysis Research Corporation, Palo Alto, California, U.S.A., FEM software, User manuals, version K2, 1986.
- [9] ten Hagen, E.A.M. Mechanische karakterisering van synthetische rubbers. M.Sc. Thesis, Eindhoven University of Technology, Jan. 1988 (in Dutch).

CHAPTER 5 : CONTACT TEMPERATURE.

5.0 OVERVIEW.

- 5.1 Introduction.
- 5.2 Thermal network model.
- 5.3 Measuring the contact temperature.
- 5.4 Numerical results.
- 5.5 Summary.
- 5.6 References.

With respect to service life, it is important to have an indication of the seal-shaft contact temperature that will occur in seal applications in practice. In this chapter a thermal network model is employed to calculate the contact temperature. Different experimental techniques are discussed to measure the contact temperature. Finally the numerical results obtained with the thermal network model are compared to the experimental results.

5.1 INTRODUCTION.

It is recommended by seal manufacturers not to use lip seals beyond a certain maximum operating temperature, depending on the composition of the seal material (for Nitrile rubber $T_{\max} \approx 90$ °C). Beyond this temperature increased wear will occur, resulting in a considerable decrease in seal service life. The contact temperature which results from a certain dissipated friction heat depends on the heat balance in the entire machine. In the next paragraph a numerical method is presented to calculate an estimate of the steady-state and transient contact temperatures that will occur.

5.2 THERMAL NETWORK METHOD.

In the thermal network method (TNM) a mechanical construction is divided into thermal components, forming a thermal network. The thermal components used in such a network are resistances, capacitors, and positive and negative heat sources. In analogy with electrical circuits, temperature corresponds to voltage and heat rate to current. Advantages of the TNM method for thermal analysis are :

- (a) the TNM is easy to conceive and very flexible because of its open

structure and (b) the TNM does not demand sophisticated software and hardware. The TNM calculations presented in this chapter can be performed on a simple (640 kilobyte) personal computer.

Nevertheless, this method has not yet been used frequently for the analysis of heat problems in mechanical engineering. The main reason for this is that there are often no adequate analytical models available to describe the different mechanical elements such as gears, bearings and seals in terms of thermal components such as resistances, capacities or heat sources.

The FEM is frequently used for analysing heat problems in mechanical engineering. A disadvantages of the FEM in comparison with the TNM is that the software and hardware are expensive.

In the present chapter a combined approach was chosen. The FEM can be used to determine thermal conductivity matrices for relatively complex machine elements, such as seals. These conductivity matrices are then incorporated into the thermal network model.

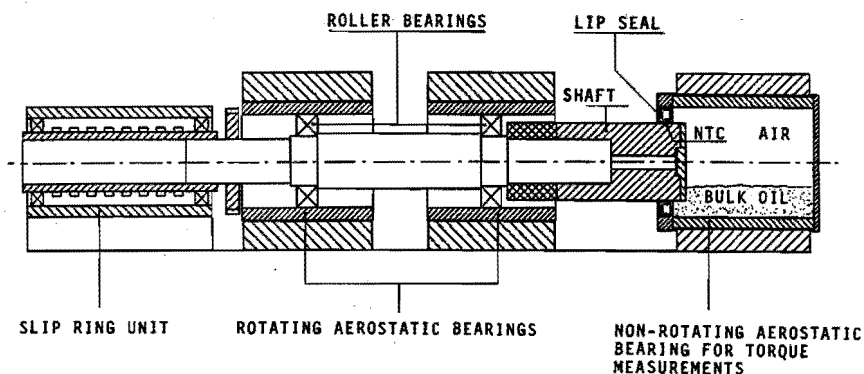


Fig. 5.1 : Sketch of temperature measurement test-rig .

The size of the conductivity matrix of a machine element depends on the number of temperatures and heat fluxes one wishes to distinguish for that element. The heat flow and the temperature distribution in the seal are assumed to depend on only 4 temperatures: (1) the seal-shaft contact temperature, (2) the temperature of the machine housing, (3) the bulk oil temperature and (4) the air temperature. The conductivity matrix of the seal therefore is a 4×4 matrix. This reduces the original 676 element FEM-mesh of the seal of chapter 4 to a simple, condensed and more efficient network component.

The thermal network model of the test-rig for temperature measurements from figure 5.1 is shown in figure 5.2, see van Ostayen [4]. A part of the test-rig on the left-hand side of the shaft was modeled by only one resistor and one capacitor. The thermal resistance and capacity of these two components have been derived from measurements. This simplification is allowed here because we are mainly concerned with the relation between the dissipated heat and the temperature in the seal-shaft contact area. The resulting network is smaller and machine elements such as the slip ring unit and the rotating air bearings do not have to be modeled.

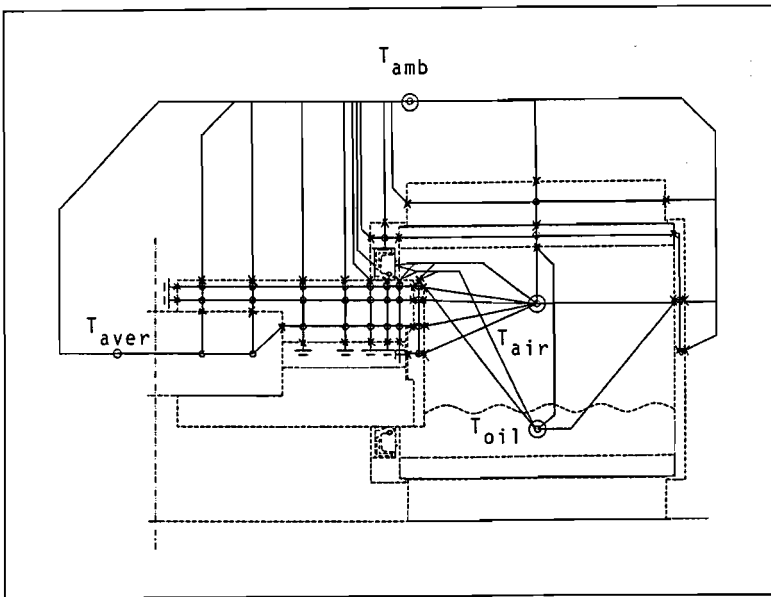


Fig. 5.2 : Thermal network model of the test-rig from fig. 5.1

- o temperature node with capacity
- x temperature node without capacity
- each line connecting nodes represents a resistor.

T_{amb} this node represents the ambient air surrounding the test-rig, it is assumed to be constant at 20 °C.

T_{oil} this node represents the average oil bulk temperature.

T_{air} this node represents the average air temperature inside the housing.

T_{aver} this node represents the average temperature of the part of the test-rig that was not modeled: the slip ring unit, the rotating aerostatic bearings and the main shaft.

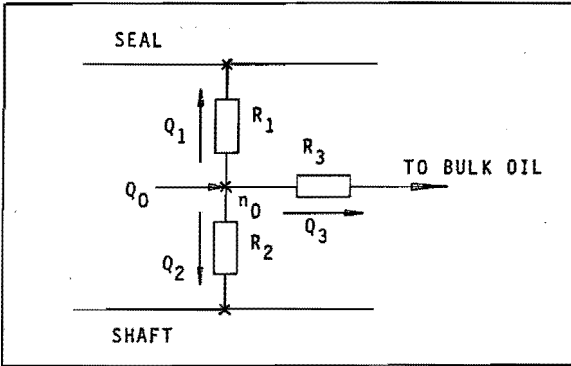


Fig. 5.3 : Detail of thermal network in the contact area.

The oilfilm between seal and shaft is assumed to have one homogeneous temperature. One node n_0 therefore suffices to describe the oilfilm, see fig. 5.3. This node is connected to the following components :

- 1) A heat source Q_0 describing the heat flow dissipated to the oilfilm.
- 2) A resistor R_1 related to the conductive heat transfer from the oilfilm to the seal. The oil flow in the oilfilm is assumed to be laminar. Then the heat transport from the oilfilm to the seal is conductive and perpendicular to the laminar flow.
- 3) A resistor R_2 related to the conductive heat transfer from the oilfilm to the shaft.
- 4) A resistor R_3 related to the heat transfer from the oilfilm to the bulk oil. A part of the heated oil in the oilfilm will be exchanged with the cooler bulk oil. The result is a heat flow from the oilfilm to the oil bulk.

The shaft under the seal is modeled by 82 resistors and 31 capacitors thus enabling a good representation of the large radial and axial temperature gradients. For reasons of simplicity a reduced number of resistors and capacitors are sketched in the shaft of fig. 5.2. The other metal elements in the construction such as the oil container and the static air bearing are modeled with less resistors and capacitors because of the very small temperature gradients within these elements.

Heat transfer by convection is calculated using the formulae from [2]. Generally these formulae are nonlinear in temperature.

The nonlinear system equations of the thermal network were solved using a standard network program mainly used by electrical engineers: SPICE-2G. It is a general-purpose circuit simulation program for steady-state or transient nonlinear analysis. Circuits may contain resistors, capacitors, independent and dependent voltage and current sources and several other electrical components. Nonlinear functions however are limited to polynomials.

5.3 MEASURING THE CONTACT TEMPERATURE.

Because of the relatively small dimensions of the contact width b (in practice $0.05 < b < 0.5$ mm) it is difficult to measure the contact temperature. Different experimental methods were employed to measure the contact temperature distribution.

- 1) NTC thermistors.
- 2) Thin film thermal transducers.
- 3) Infra-red temperature measurements.

NTC thermistors are reliable, relatively cheap, commercially available temperature sensors (accuracy ± 1 °C). A disadvantage of these thermistors is that because of their diameter ($d = 2$ mm) only an average contact temperature can be measured in a bandwidth which is much larger than the actual contact width.

Therefore attempts were made using a Titanium thin film micro-transducer, which was evaporated on the shaft surface, see figure 5.4. Because of the small dimensions of these sensors (width = $10 \mu\text{m}$, length = $600 \mu\text{m}$, height = $1 \mu\text{m}$) and their accuracy (± 0.5 °C) they seemed very useful for measuring the contact temperature (distribution) under the lip. In order to measure the temperature profile in the contact area the seal was translated in axial direction over the transducer on a rotating shaft. Problem here was that each time the seal was translated, the torque changed, probably because the seal encountered a different local roughness pattern on the shaft, which resulted in a change of dissipated friction heat and in small fluctuations of the contact temperature of ± 2 °C. This temperature fluctuation was too large to obtain a valid temperature profile within the contact area. Disadvantages of these micro-transducers sensors are (a) that due to wear they have a limited service life (approximately 2 hours) which is short compared to the transient times before the contact temperature has reached a steady state (approximately 1.5 hours), and (b) that the shaft surface had to be polished (locally) before evaporation, resulting in a local change of shaft roughness, and thus in a change of torque.

In order to obtain an integral temperature profile of the contact temperature of the seal lip contact surface, infra-red temperature measurements were performed via a mirror and a small cylindrical glass window (diameter = 2 mm, length = 1 mm), in a fixed hollow steel shaft. The temperature profile measured at 3 different seal angular velocities is represented in figure 5.6. The infra-red measurement technique is based on determining temperature differences (resolution 0.5 °C). However, an accurate determination of the absolute temperature is difficult with this technique without a reference temperature.

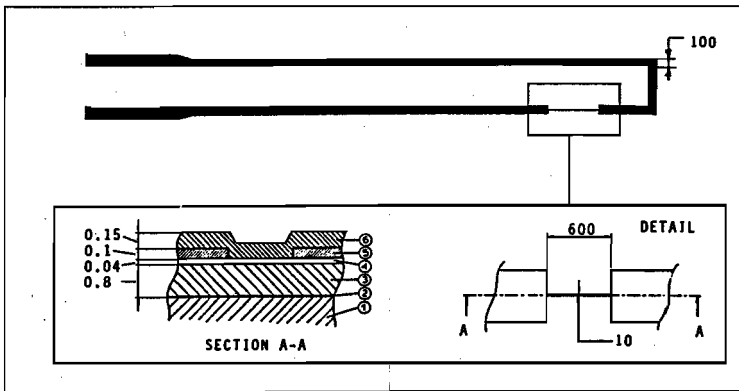


Fig. 5.4 : Thin film thermal microtransducer (dimensions are in microns). (1) substrate (shaft), (2) adhesive layer of Ti, (3) insulating layer of Al_2O_3 , (4) transducer of Ti, (5) conductor pattern of Au, (6) protective layer of Al_2O_3 , see [3].

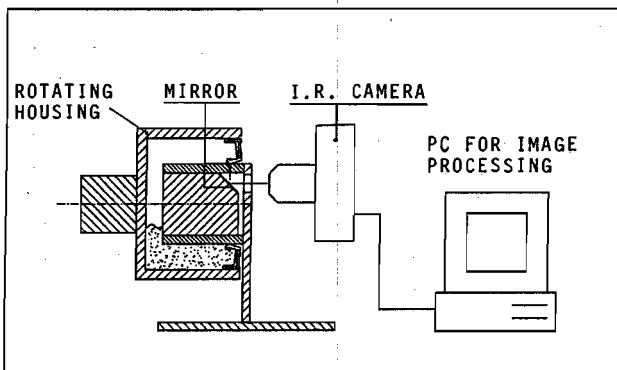


Fig. 5.5 : Sketch of test-rig for infra-red temperature measurements.

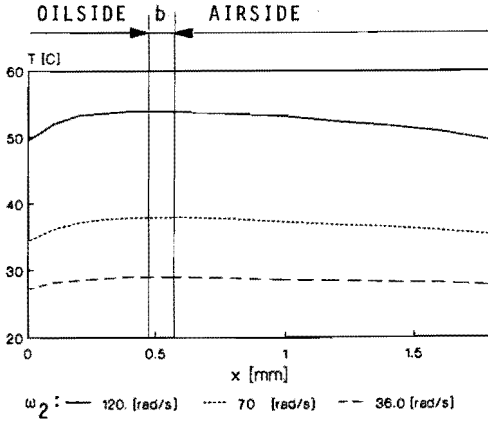


Fig. 5.6 : Temperature distribution for different seal angular velocities, measured using the infra-red technique.

5.4 NUMERICAL RESULTS.

The results are valid for the test-rig of figure 5.1, where the non-rotating shaft was immersed in Shell Tellus 46 oil, over an angle of 0.68 rad of the shaft circumference. The ambient air temperature was held constant at $T = 20$ °C.

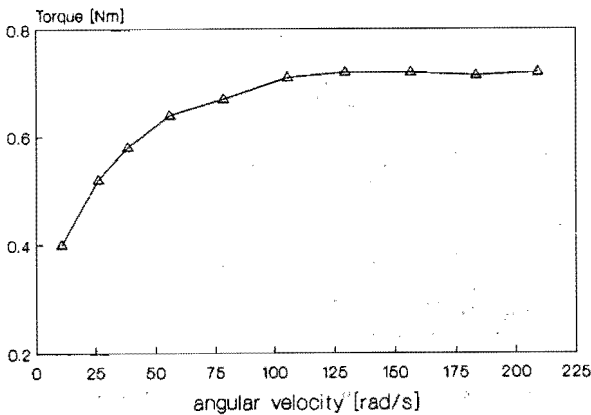


Fig. 5.7 : Steady-state seal torque as function of the shaft angular velocity as measured on the test-rig.

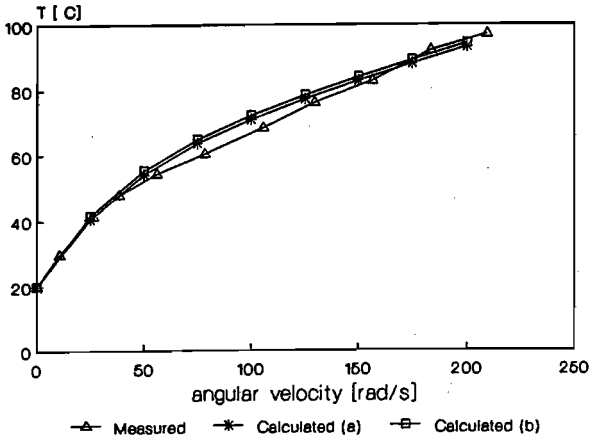


Fig. 5.8 : Steady-state seal-shaft contact temperature as function of the shaft angular velocity corresponding to seal torque in fig. 5.7.

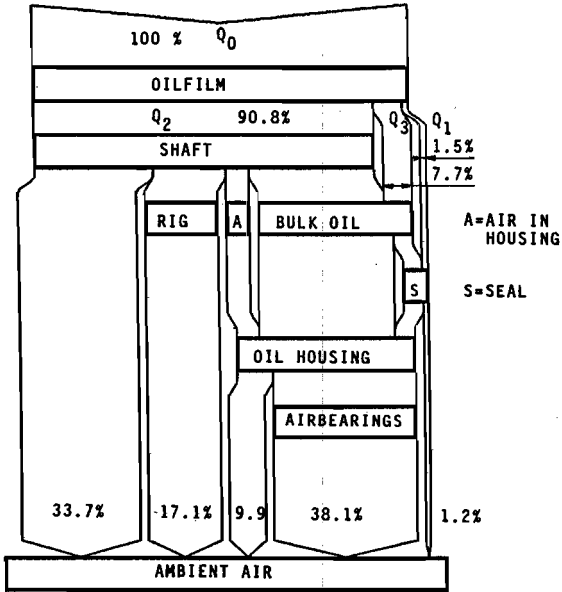


Fig. 5.9 Sankey-diagram of the heat flows in the test-rig as calculated with the TNM. $\omega = 125$ rad/s and $T = 0.72$ Nm, thus $Q_0 = T \cdot \omega = 90$ W.

The torque was measured as function of the shaft angular velocity, see fig 5.7. Figure 5.8 shows the steady-state contact temperatures measured with the thermistors, corresponding to the torque of figure 5.7. In the same figure are sketched the steady-state contact temperatures as calculated with the TNM, for 2 situations : (a) with the seal taken into account and (b) without the seal taken into account in the network model.

In situation (a) the seal was incorporated into the TNM as a 4x4 conductivity matrix as determined by the FEM. This results in a heat flow as represented in figure 5.9.

In situation (b) the heat transfer through the seal was eliminated by giving the seal a very high resistance (if $R_1 = \infty$ then $Q_1 = 0$). From figure 5.8 it can be seen that the presence of the seal as a thermal component has only a very minor influence on the calculated contact temperatures. Therefore it can be concluded that the seal does not necessarily have to be taken into account in the network. This simplification eliminates the use of the FEM analysis to determine the seal conductivity matrix, which means a considerable reduction in modeling time.

Figure 5.10 shows transient contact temperatures at a constant shaft angular velocity for situation (b).

The practical utility of the TNM is illustrated by the good correspondence between measured and calculated results for both steady-state and transient situations.

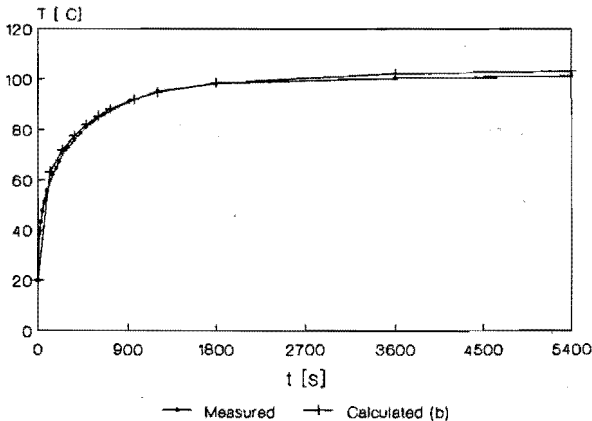


Fig 5.10 Transient contact temperatures for $\omega = 204.2$ rad/s and a steady-state torque $T = 0.82$ Nm. The steady-state torque was reached after 900 seconds.

5.5 SUMMARY.

- 1) To calculate the seal-shaft contact temperature resulting from a certain dissipated friction heat rate the heat balance of the entire machine has to be taken into account.
- 2) The thermal network method provides a useful tool to model the heat balance of the machine and to calculate transient and steady-state seal-shaft contact temperatures.
- 3) The heat transfer through the seal has only a very minor influence on the contact temperature.
- 4) Accurate experimental determination of the contact temperature is difficult due to the small dimension of the seal-shaft contact width.

ACKNOWLEDGEMENT.

The author would like to thank mr. B. Munneken from the CFT department of Philips Eindhoven for performing the infra-red temperature measurements.

5.6 REFERENCES.

- [1] Upper, G. Dichtlippentemperatur von Radial-Wellen Dichtringen. Thesis university of Karlsruhe, Germany, 21 July 1967. (In German)
- [2] Wong, H.Y. Handbook of essential formulae and data on heat transfer for engineers, Longman, London and New York, 1977.
- [3] van Leeuwen, H; Meyer, H; Schouten, M.J.W. Elastohydrodynamic film thickness and temperature measurements in dynamically loaded concentrated contacts: eccentric cam-flat follower. Proc. 13th Leeds-Lyon Symposium on Tribology, University of Leeds, 8-12 sept. 1986.
- [4] van Ostayen, R.A.J. Het gebruik van de thermische netwerkmethodie bij de beschrijving van de warmtehuishouding van werktuigbouwkundige constructies. M.Sc. thesis, Eindhoven University of technology, August 1988. (in Dutch)
- [5] Verfuurden, P.H.M. Bijdrage aan het onderzoek naar de werking van radiale lipafdichtingen. Internal report, Eindhoven University of technology, June 1988. (in Dutch)

CHAPTER 6 : THE PUMPING MECHANISM, A MODEL.

6.0 OVERVIEW.

- 6.1 Introduction.
- 6.2 Principles of the visco-seal concept.
- 6.3 Model definition.
- 6.4 Discretization of the problem.
- 6.5 Discussion of the results.
- 6.6 Summary.
- 6.7 References.

In this chapter a model is presented to describe the active pumping action of radial lip seals. On basis of the visco-seal concept, the elastohydrodynamic film pressure distribution under the lip in the seal-shaft contact is calculated.

6.1 INTRODUCTION

Proper functioning radial lip seals exhibit a active pumping action: they are able to pump oil from the airside to the oilside of the seal. In literature on radial lip seals a number of hypotheses are presented to describe this pumping action, see [1]. An interesting hypothesis was proposed by Kammüller [2] in 1986. Observing the worn contact area of seals via a scanning electron microscope, he noticed that after a short run-in period, small axially extended wear grooves were formed. Kamüller studied the worn seals in a dismantled position, thus the seals were not in a pre-stressed radially deformed state.

Figure 6.1 shows the groove pattern in radially deformed state corresponding to the mounting position of the seal on a fixed shaft, visualized using a transparant perspex prismatic torus, as presented in figure 6.2.

By evaporizing a thin gold marker line on the seal contact area in axial direction, Kammüller observed through a rotating hollow perspex shaft, that the seal contact area is tangentially deformed during shaft rotation, due to shear forces. Kammüller assumed that the tangentially deformed groove patterns form a pair of counteracting visco-seals causing a deviation of the tangential shear flow in the seal-shaft contact area, resulting in a net flow towards the oilside of the seal.

The model presented in this chapter is based on this visco-seal concept.

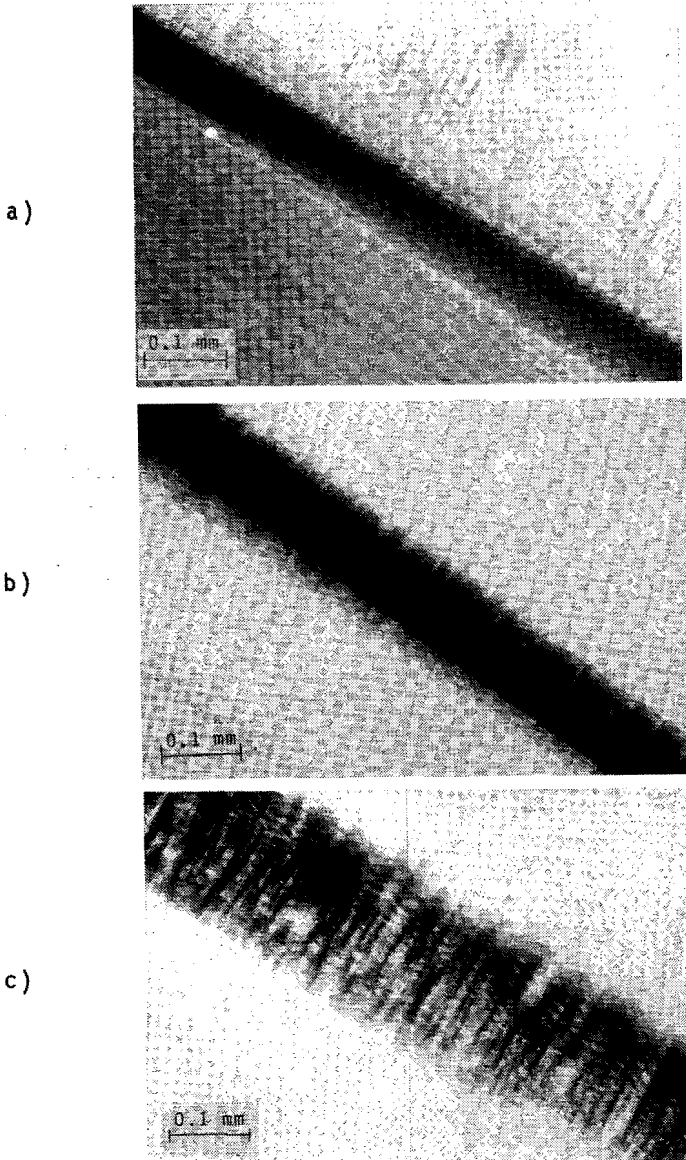


Fig. 6.1 : Seal contact zone in radially deformed state (under dry, static conditions), photographed through a microscope and a prismatic torus: a) virgin seal, b) wear pattern after 5 minutes and c) wear pattern after 90 hours service life at shaft angular velocity 125.6 rad/s in Shell Tellus 46 oil.

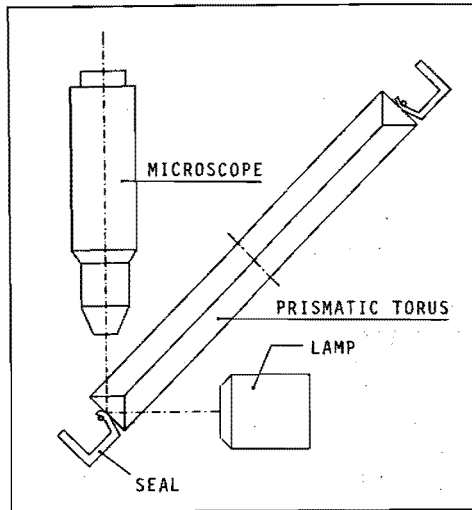


Fig. 6.2 : Set up of the prismatic torus and the microscope used to visualize the deformed contact area. Where the seal is not in contact with the perspex, total internal reflection of the light occurs, resulting in bright area's in the microscope image. Where the seal is in contact, the frustated total internal reflection results in dark area's.

6.2 PRINCIPLES OF THE VISCO-SEAL CONCEPT.

The principles of the visco-seal concept are represented in figure 6.3. On the airside the pumping action causes a drop in pressure Δp , which is counterbalanced by a drop in pressure over the oil-air interface on the airside of the seal, see chapter 2.

Boon and Tal [3] have formulated a model to describe the sealing mechanism for a pair of counteracting visco-seals. In their model they assumed constant groove angles ϕ_1 and ϕ_2 . In case of lip seals the groove angles are not constant, but they vary as function of the location x in the contact area. The local groove angle $\phi(x)$ is determined by the tangential deformation of the contact area of the seal. The tangential deformation is determined by the tangential stiffness of the seal and the tangential shear stress distribution acting on the contact area.

6.3 MODEL DEFINITION.

Our aim is to calculate the elasto-hydrodynamic pressure distribution $p(x)$ in the contact area, caused by the deformed groove pattern in the seal-shaft contact area. The following assumption are made :

- 1) The visco-seal mechanism is the governing pumping mechanism.
Probably the pumping mechanism is not based on one single concept, but on a number of physical processes acting simultaneously such as the cascade pumping effect, see Müller [1], and the effects of axial reciprocating lip motion, Horve [4].
- 2) The problem is isothermal.
- 3) Only steady-state situations are considered.
- 4) Shaft and seal are rotating co-axial, there is no relative velocity component in axial or radial direction, and the problem is assumed to be axisymmetric.
- 5) The shaft surface and the seal surface apart from the grooves are perfectly flat.

On basis of the Navier-Stokes equations Boon and Tal [3] derived a model to describe the pressure distribution in concentrically operating visco-seals with rigid rectangular grooves. Using the visco-seal model from [3] it can be derived that for the first derivative of the pressure can be written :

$$\frac{dp}{dx} = \frac{3 \eta \omega d}{s^2} \frac{t u (1-u)(w-1)(w^3-1)}{(1+t^2)w^3 + t^2 u(1-u)(w^3-1)^2} \quad (6.1)$$

where :

$$u = \frac{e}{a+e} \quad ; \quad w = \frac{s+c}{s} \quad ; \quad t = \tan\left(\frac{\pi}{2} - \phi(x)\right)$$

$$\phi(x) = \arctan \frac{dv}{dx}$$

- a = Width of ridge
- b = Contact width
- c = Height of groove
- d = Diameter shaft
- e = Width of groove
- s = Gap height
- η = Dynamic viscosity of oil
- v = Tangential displacement field.

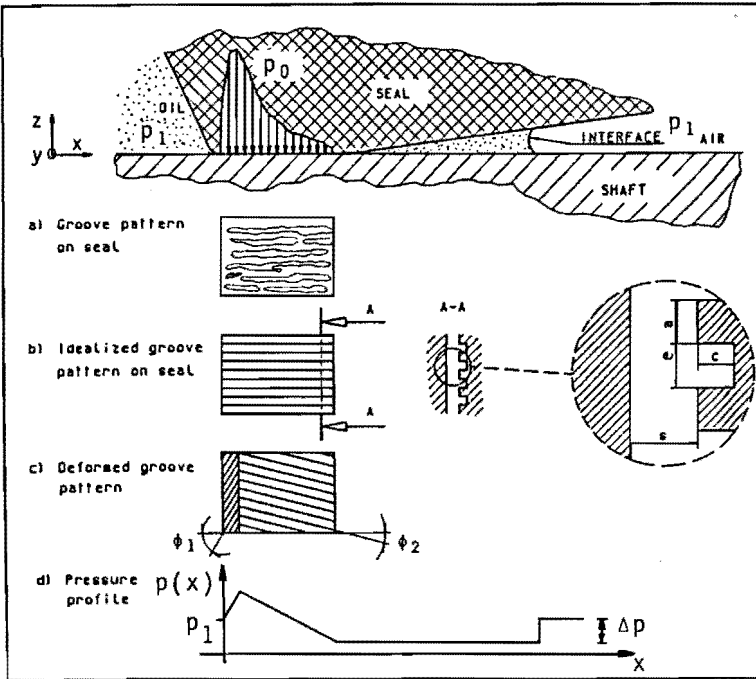


Fig. 6.3 : The visco-seal concept.

Friction in lubricated rubber-steel contacts is a complex mechanism, governed by many parameters. In most of the literature on radial lip seals it is assumed that the friction mechanism for radial lip seals is based on simple shear in a Newtonian fluid for a laminar Couette flow between concentrically rotating cylinders. On basis of accurate torque, contact area and contact temperature measurements the author found very low calculated average film height values \bar{h} ($\bar{h} < 0.1 \mu\text{m}$) when assuming a situation of simple shear. These average filmheight values \bar{h} were approximately 10 times as small as the Ra roughness of the shaft measured in tangential direction. This raised doubts about the reliability of the simple shear model. Therefore the following Coulomb-like friction model will be proposed here to describe the shear stresses τ acting on the seal contact area.

$$\tau = f \cdot (p_0 - p) \quad (6.2)$$

Where : p_0 = static contact pressure distribution.
 p = elastohydrodynamic pressure distribution.
 f = friction coefficient.

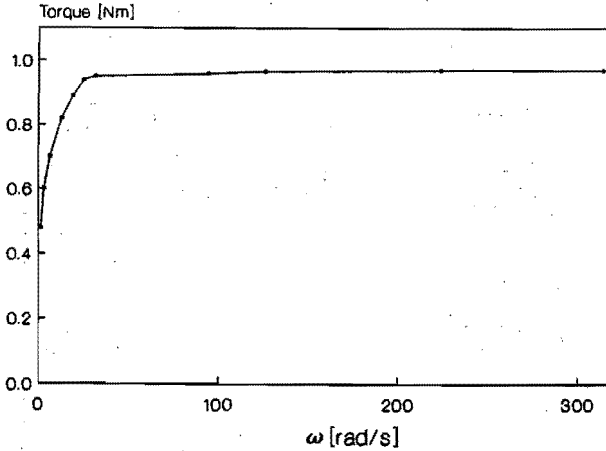


Fig. 6.4 : Steady-state friction torque $T_m = T_m(\omega)$.

The seal torque T is equal to the shear stresses integrated over the contact area :

$$T = \int_0^b \tau \pi d dx \quad (6.3)$$

In practice T is not constant, but a function of the shaft angular velocity ω . Figure 6.4 shows a plot of the friction torque $T_m(\omega)$ as measured on a test-rig. The friction coefficient $f=f(\omega)$ is now defined by equation (6.4) :

$$T_m(\omega) - \pi \cdot d \cdot f(\omega) \cdot \int_0^b (p_0 - p(\omega)) \cdot dx = 0 \quad (6.4)$$

The relation between the shear-stress distribution τ and the tangential displacements field v is described by the operator K_T , representing the seal stiffness in tangential direction, where :

$$\tau = K_T v \quad (6.5)$$

Equations (6.1),(6.2),(6.4) and (6.5) describe the problem to be solved. Analytical solution of this set of equations is not possible. Therefore the problem was solved numerically by discretization.

6.4 DISCRETIZATION OF THE PROBLEM.

A finite element method (FEM) model was used to determine a discrete form of the stiffness of the seal contact area in tangential direction in the form of a tangential stiffness matrix K_T . K_T can be achieved via the finite element method through static condensation, or through nodal perturbation. The most elegant of the two methods, static condensation can be used to reduce the number of element degrees of freedom, by condensating out the non-relevant degrees of freedom, see [5], pag 450. Because the stiffness matrix of the complete structure (the seal) could not be obtained directly from the FEM program the nodal perturbation technique was chosen.

Because the FEM program ABAQUS (version 4.5), which was also used in chapter 3, did not provide hybrid axi-symmetric torsional elements, the MARC (version K2) program was used. The MARC FEM model contained 355 4-node linear, hybrid constant pressure, axisymmetric ring, torsional elements, [8]. In the FEM model the mechanical behaviour of the rubber material was approximated using the Mooney-Rivlin model (see chapter 3).

First the seal was deformed (pre-loaded) according to the interference fit of the seal on the shaft. This results in a static pressure distribution p_0 . Using MARC for the calculation of the nonlinear static pre-load, numerical convergence problems occurred using the interface elements from MARC. These problems did not occur using ABAQUS, which is in many ways very similar to MARC, but which provides rigid surface interface elements [9], that did not show convergence problems. The radial displacements of the nodes in the contact area as calculated with ABAQUS were used as an initial fixed radial displacement input for the MARC model. The MARC static contact stress distribution, calculated with the fixed displacement input was checked and was identical to the ABAQUS results. Using this pre-deformed state as an initial condition the nodal perturbation technique was executed on the MARC model. A tangential displacement of $1 \mu\text{m}$ was successively applied to each of the 10 nodes in the seal contact width b ($b = 0.075 \text{ mm}$), and the corresponding nodal reaction forces were calculated. During this procedure only tangential displacements were considered, radial displacements were set to zero and axial displacements were set free.

Using the nodal perturbation technique it was assumed that because of the relatively small deformations in tangential direction, the tangential stiffness matrix is linear, thus $K_T \neq K_T(v)$.

With the calculated nodal reaction forces corresponding to the nodal perturbations we have obtained the tangential stiffness matrix \underline{K}_T , where \underline{K}_T is a 10 x 10 symmetric, positive definite matrix linking nodal force vector \underline{F}_T to the nodal displacements vector \underline{y} . For equations (6.1), (6.2), (6.4) and (6.5) we now write the following non-linear set of equations :

$$\underline{K}_T \underline{y} - \underline{F}_T = 0 \quad (6.6a)$$

$$T_m - \pi \cdot d \cdot f \int_0^b (p_0 - p) \cdot dx = 0 \quad (6.6b)$$

where

$$\begin{aligned} \underline{F}_T &= G \tau = G f(p_0 - p) = G f(p_0 - I \frac{dp}{dx}) = G f(p_0 - I J \phi) \\ &= G f(p_0 - I J M \underline{y}) \end{aligned}$$

and

- \underline{F}_T = nodal force vector
- G = linear integral operator to transform the continuous shear stress distribution to a nodal force vector.
- I = linear integral operator to transform $\frac{dp}{dx}$ to p .
- J = non-linear operator to transform groove angle ϕ to $\frac{dp}{dx}$.
- M = non-linear differential operator to transform tangential displacements \underline{y} to groove angle ϕ .

The unknown variables \underline{y} and f are now solved for a certain value of ω by substituting $T_m = T_m(\omega)$ in (6.6b) and then solving (6.6a) and (6.6b) by a Newton-Raphson iteration scheme.

Note that in the model described above, full film lubrication will only occur when $p > p_0$. This is caused by the assumption that the shaft surface and the seal surface apart from the grooves is perfectly flat. In practice the micro-roughness of the shaft will cause microasperity lubrication effects. Apart from this the filmheight is also determined by visco-elastic and inertial properties of the seal lip, because in most practical situations the seal lip will not be able to follow the small-amplitude oscillatory movements of the shaft surface caused by eccentricity or out of roundness of the shaft, see chapter 8. The model described above should therefore merely be considered as a qualitative model to describe the pumping action.

The values of the parameters as used in this chapter are listed in table 6.1.

Width of ridge	a =	5	μm
Contact width	b =	75	μm
Height of groove	c =	0.5	μm
Width of groove	e =	10	μm
Gap height	s =	1	μm
Diameter shaft	d =	70	mm
Dynamic viscosity oil	$\eta =$	0.023	Pa.s
Vapour pressure oil (T=50°C)	$p_v =$	10	kPa
Ambient pressure	$p_1 =$	100	kPa

Table 6.1 : Numerical values of the parameters.

6.5 DISCUSSION OF THE RESULTS.

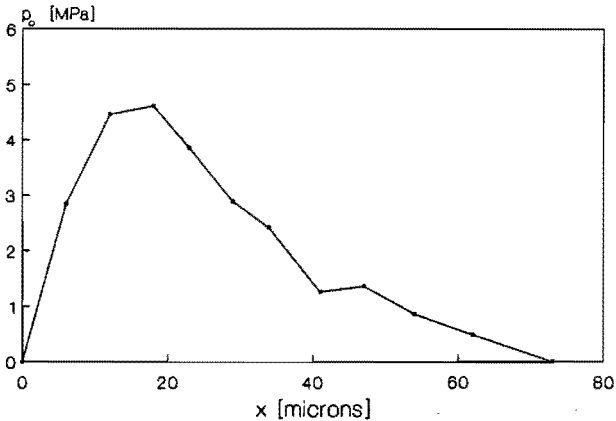


Fig. 6.5 : Static pressure profile.

1) Figure 6.5 shows the nonsymmetric static contact pressure profile p_0 as calculated with the FEM. The maximum in p_0 occurs on the oilside of the seal. The author did not succeed in measuring the pressure profile in the small contact width. The non-symmetric profile of the contact pressure is a necessary condition for the pumping action.

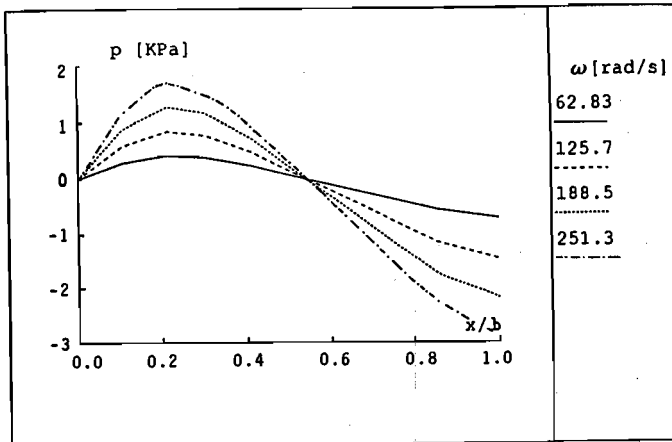


Fig. 6.6 : Elastohydrodynamic pressure profile p caused by the tangentially deformed groove pattern in the seal contact area.

The values of the parameters are listed in table 6.1

$$\Delta p = p(x/b=0) - p(x/b=1) = p_1 - p(x/b=1).$$

2) Figure 6.6 shows the elastohydrodynamic pressure profile p for different values of ω calculated with the model described above. Note that on the airside edge of the contact area $p < p_1$. Here the seal is sucked to the shaft surface. This low pressure region on the airside was also found experimentally by Shimotsuma and Iwasaki, [7].

3) Fig 6.6 also shows that when ω increases, Δp increases. This explains the axial movement of the meniscus as experimentally found in chapter 2.

4) In our model it is assumed that cavitation will only occur when $p < p_v$, where p_v is the vapour pressure of oil. Using the parameters from table 6.1 no cavitation was found. Note that p in our model is an overall-pressure. In practice cavitation can also occur for $p > p_v$ especially in regions with a relatively low p value (such as the edges of the contact area and particularly the airside edge where p reaches the lowest values), due to microasperity cavitation at the divergent side of asperities, see [10].

5) Figure 6.7 shows the tangential deformation of the contact area due to the shear forces. This tangential deformation shows a good (qualitative) correspondence with the deformation field experimentally observed by Kammüller [2].

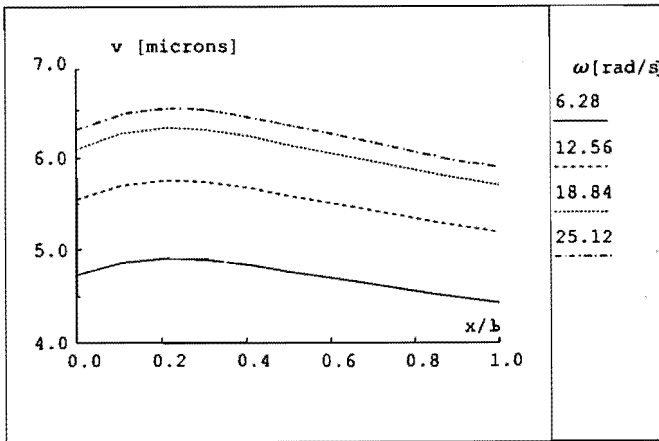


Fig. 6.7 : Tangential displacement field v .

6.6 SUMMARY.

- 1) The visco-seal model as described in this chapter gives insight into the active pumping mechanism of radial lip seals.
- 2) The model described in this chapter explains the axial movement of the oil-air interface and the occurrence of a low pressure region on the airside edge of the contact area.
- 3) The quantitative value of the models as described above is limited because in practice the seal pumping mechanism is probably based on (a complex interaction of) a number of different physical processes.

6.7 REFERENCES

- [1] Müller, H.K. Concepts of sealing mechanism of rubber lip type rotary shaft seals. Proc. BHRA 11th Int. Conf. on Fluid Sealing (1987) Paper K1.
- [2] Kammüller, M. Zur Abdichtwirkung von Radial-Wellendichtringen. Thesis Univ. of Stuttgart, August 18, 1986 (In German).

- [3] Boon, E.F.; Tal, S.E. Hydrodynamische Dichtung für rotierende Wellen. Chemie-Ing.-Techn., 31. Jahrg. 1959, No. 3, pp 202-212 (In German).
- [4] Horve, L. A macroscopic view of the sealing phenomenon for radial lip seals. BHRA Intern.Conf. on Fluid Sealing 1987, Paper K2
- [5] Bathe, KJ. Finite Element Procedures in Engineering Analysis. Prentice-Hall, Inc., Englewood Cliffs, New Jersey 07632, 1982.
- [6] Stakenborg, M.J.L. On the sealing mechanism of radial lip seals. To be published in Tribology International.
- [7] Shimotsuma, Y.; Iwasaki, M. Study on lip type oil seals (1), characteristics of pressure distributions. Journal Japanese society of Lubr. Eng. volume 19, december 1974 (In Japanese, summary and remarks in English)
- [8] MARC Analysis Research Corporation, Palo Alto, California, U.S.A., FEM software, User manuals, version K2, 1986.
- [9] Hibbit, Karlson and Sorensen. ABAQUS FEM software, user manuals, version 4-5
- [10] Hamilton, D.B.; Walowit, J.A.; Allen, C.M. Microasperity lubrication. Journal of Basic Engineering, 1968, pp 351-355.

CHAPTER 7 : LEAKAGE, A MODEL.

7.0 OVERVIEW.

- 7.1 Introduction.
- 7.2 Model definition.
- 7.3 Numerical results.
- 7.4 Summary.
- 7.5 References.

In chapter 6 attention was focussed on the sealing mechanism of radial lip seals. A question still to be answered is, why do seals start leaking. In this chapter a model is presented which describes leakage as a result of a breakdown of the oil-air interface on the airside of the seal, in consequence of centrifugal forces acting on the oil. The model predicts that leakage will occur for $\omega > \omega_{\text{leak}}$, where ω_{leak} depends on the pumping pressure Δp of the seal.

7.1 INTRODUCTION.

Explanations or hypotheses for seal leakage are scarce. Prati [1] experimentally observed the occurrence of clearances between a seal and an eccentric whirling shaft. At higher whirling frequencies the viscoelastic seal material prevented a complete rebound of the seal, resulting in oscillating clearances between seal lip and shaft surface.

Prati assumed that these oscillating clearances between shaft and seal are responsible for leakage, but he did not discuss the leakage mechanism.

7.2 MODEL DEFINITION.

The leakage model presented here is based on the assumption that centrifugal forces on the oil in the clearance between seal and shaft can cause a breakdown of the interface on the airside of the seal. For a certain angular velocity the interface can no longer be closed across the clearance. The pressure difference across the clearance in consequence of centrifugal forces then becomes so high that the

surface tension is no longer able to prevent a breakdown of the interface. A breakdown of the interface then occurs, resulting in leakage. Based on this assumption Bootsma [2] has formulated a leakage criterion for the breakdown of an oil-air interface in a plain section at the end of a concentrically operating spiral-groove bearing. Bootsma found a good correspondence between the numerical results obtained with his leakage model and experimental results of leakage tests performed on spiral-groove bearings. In case of radial lip seals the clearance between seal and shaft is not plain, but curved. In appendix A3 a model is derived for the breakdown of an oil-air interface on a curved section.

7.3 NUMERICAL RESULTS.

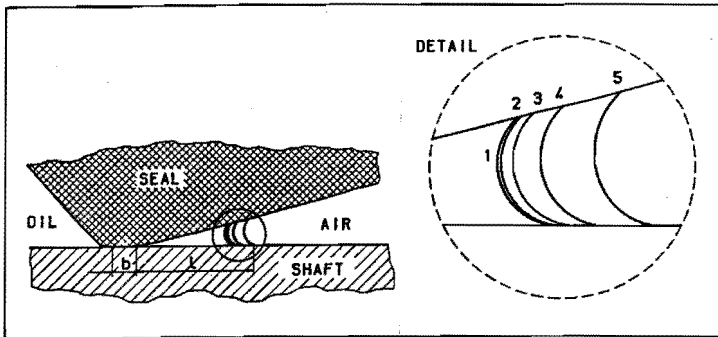


Fig. 7.1 : Shape and location of the oil-air interface for different values of the shaft angular velocity ω_1 , at a constant seal pumping pressure $\Delta p = 1$ kPa. ($b = 0.075$ mm)

- 1) $\omega_1 = 0.0$ rad/s (0.Hz)
- 2) $\omega_1 = 157.1$ rad/s (25.Hz)
- 3) $\omega_1 = 314.2$ rad/s (50.Hz)
- 4) $\omega_1 = 471.2$ rad/s (75.Hz)
- 5) $\omega_1 = 628.3$ rad/s (100.Hz)

Figure 7.1 shows the shape and location of the oil-air interface for different shaft angular velocities ω_1 , at a constant value of the seal pumping pressure Δp , as calculated using the model of appendix A2. Figure 7.2 shows the shape and location of the meniscus for different values of the pumping pressure Δp at a constant shaft rotational frequency ω_1 . Figures 7.1 and 7.2 illustrate that $l = l(\omega, \Delta p)$. In appendix A2 a leakage criterion is formulated, which says that there is a certain minimum pumping pressure $\Delta p_{\min} = \Delta p_{\min}(\omega)$ needed to prevent leakage. Figure 7.3 shows Δp_{\min} for a rotating shaft ($\omega_1 \neq 0$ and $\omega_2 = 0$) and for a rotating seal ($\omega_1 = 0$ and $\omega_2 \neq 0$).

Because at this moment the function $\Delta p = \Delta p(\omega)$ is still unknown and could not be measured a quantitative verification of the leakage model presented in this chapter was not yet possible.

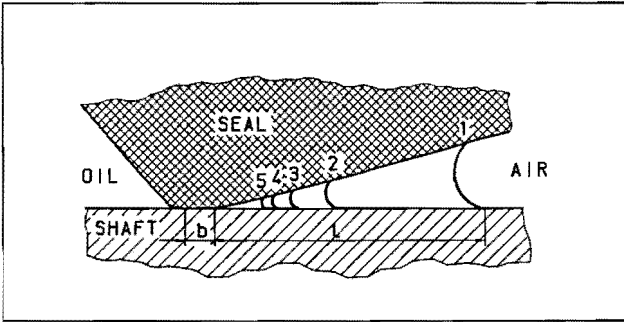


Fig. 7.2 : Shape and location of the oil-air interface for different values of the seal pumping pressure Δp , at a constant shaft angular velocity $\omega_1 = 314.2 \text{ rad/s}$ (50 Hz).

- 1) $\Delta p = 0.5 \text{ kPa}$ 2) $\Delta p = 1.5 \text{ kPa}$
- 3) $\Delta p = 2.0 \text{ kPa}$ 4) $\Delta p = 2.5 \text{ kPa}$
- 5) $\Delta p = 3.0 \text{ kPa}$

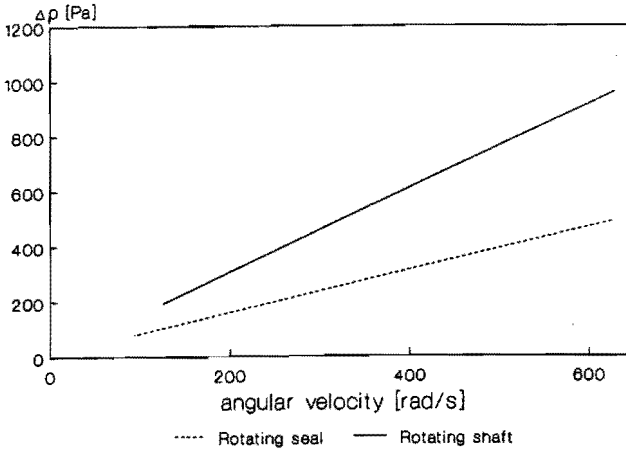


Fig 7.3 : Minimum pumping pressure $\Delta p_{\min} = \Delta p_{\min}(\omega)$ to prevent leakage for a rotating shaft and for a rotating seal.

7.4 SUMMARY.

- 1) Seal leakage is explained on basis of a breakdown of the oil-air interface due to centrifugal forces acting on the oil in the airside gap between the seal and shaft.
- 2) To prevent a breakdown of the oil-air interface a minimum seal pumping pressure is needed, which depends on the shaft (or seal) angular velocity.

The leakage model assumes a proper functioning, pumping seal on a perfectly flat shaft. In practice leakage can be based on many other principles, e.g. due to damage of the seal lip, due to a loss of contact pressure (wear), due to converse installation of the seal, or due to an outward pumping action of spiral turning grooves on the shaft.

7.5 REFERENCES.

- [1] Prati, E. A theoretical-experimental method for analyzing the dynamic behaviour of elastomeric radial lip seals. Rubber Chemistry & Technology, 60, 1987 no 1., pp176-189.
- [2] Bootsma, J. Liquid-lubricated spiral-groove bearings. Thesis, Delft university of technology, The Netherlands, 19 Nov. 1975.

CHAPTER 8 : VISCO-ELASTOHYDRODYNAMIC LUBRICATION, A MODEL.

8.0 OVERVIEW.

- 8.1 Introduction.
- 8.2 Dynamic behaviour of rubber.
- 8.3 Dynamic behaviour of the seal.
- 8.4 FEM model of the seal.
- 8.5 Transfer function of the seal.
- 8.6 Interaction between fluid film and viscoelastic seal.
- 8.7 Discussion.
- 8.8 Conclusions.
- 8.9 References.

In chapters 6 and 7 the sealing mechanism was studied. Chapter 8 will concentrate on the lubrication mechanism. First, attention is paid to the mechanical behaviour of synthetic rubber under an oscillating load. Next, numerical results of a FEM analysis of the seal-shaft contact under dynamic conditions are presented. It is shown that clearances develop due to viscoelastic and inertial seal material behaviour. Finally, it follows from a short bearing model that these viscous and inertial effects can lead to a phenomenon which is designated visco-elastohydrodynamic (VEHD) lubrication.

8.1 INTRODUCTION.

In the literature on radial lip seals a lot of attention has been paid to the parallel surface lubrication mechanism of the seal lip and rotating shaft, but even until now the principles of the lubrication mechanism are poorly understood. Hirano and Ishiwata [1] have shown that the origin of the friction of seals is hydrodynamic (or mixed) lubrication, and that the seal material behaviour is viscoelastic. Their basic concept employs foil bearing theory to explain the lubrication of surface asperities, so their theory is a microasperity lubrication theory. There is no obvious reason for a macro elastohydrodynamic (EHD) lubrication mechanism under these circumstances. Nevertheless, experimental seal torque and wear studies indicate a full film lubrication mechanism, see e.g. Jagger [2]. In most of the literature on radial lip seals a static state of deformation in the seal lip is assumed. However, in practice a dynamic excitation of the seal lip occurs due to out of roundness of the shaft

or motions of the shaft center which result in an oscillatory motion of the seal lip. Beyond a certain frequency the seal lip is not able to follow the radial motions of the shaft surface, due to the viscoelastic material behaviour of the rubber seal material. Under these conditions oscillating clearances may occur between the seal lip and the shaft, as experimentally observed by Prati [3].

Prati also developed a simple three parameter solid model as a description of the entire seal structural behaviour, taking linear viscoelasticity and a lumped mass into account. He finds that clearances between the shaft and seal may occur in certain frequency bands, but the fluid film is ignored in his model. Gawlinski and Konderla [4] solved the dynamic dry contact problem of a radial lip seal by a FEM approach, where linear viscoelastic seal behaviour and a garter spring mass were taken into account.

The first part of the present chapter deals with the characterization of the dynamic seal behaviour, resulting in a transfer function of the seal. Using a FEM model, the linear viscoelastic seal response was calculated on a small-amplitude harmonic displacement input, superimposed on a nonlinear pre-stressed state. The FEM model also takes into account the inertia of the seal material and the garter spring.

In the second part of this chapter the interaction of the viscoelastic seal deformation and the fluid film formation is studied. It will be explained how visco-elastohydrodynamic (VEHD) lubrication can develop from the viscoelastic and inertial behaviour of the seal. This is exemplified by a case of periodic excitation through a whirling shaft.

8.2 RUBBER MATERIAL BEHAVIOUR UNDER DYNAMIC LOAD.

As already mentioned in chapter 3, synthetic rubbers exhibit a non-linear thermo-viscoelastic material behaviour. Applying a sinusoidal load to a rubber specimen, a material stiffness is found which depends on the amplitude of the load, the temperature of the specimen and the frequency of the load. For small-amplitude oscillating loads the influence of the amplitude of the load on the material stiffness can be neglected, then the material behaves linear thermo-viscoelastic. In figure 8.1 the linear dynamic stiffness of Nitrile rubber is represented as a function of the excitation frequency, for different temperatures. It is important to note from figure 8.1 that :

- 1) At higher frequencies the dynamic material rubber stiffness can be decades higher than the stiffness at lower frequencies.

- 2) For static conditions, and for relatively low and high frequencies the influence of temperature on the dynamic material stiffness is small.
- 3) In the frequency range $0.01 < f < 100$ Hz. temperature has a strong influence on the dynamic material stiffness.

The question arises how the frequency dependent stiffness of the seal material influences the seal-shaft contact conditions, such as the contact stress distribution. To answer this question it is necessary to study the dynamic behaviour of the entire seal.

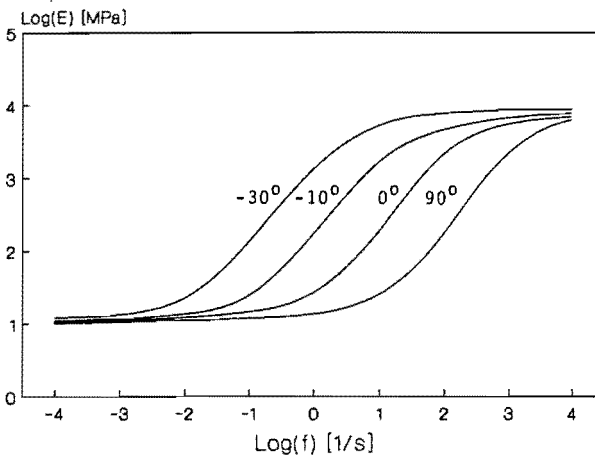


Fig 8.1 : Schematic drawing of the linear dynamic stiffness of Nitrile rubber as function of the excitation frequency at different temperatures.

8.3 DYNAMIC BEHAVIOUR OF THE SEAL.

The seal geometry and seal deformation is assumed to be axisymmetric. Figure 8.2 represents the seal as a black box system characterized by its impulse response function $h(t, \xi)$. The input signal $x(t, \xi)$ represents the axisymmetric shaft surface displacement in radial direction. The output signal is the local contact pressure $p(t, \xi)$, where coordinate ξ represents the axial position in the contact area of the seal, see Figure 8.3. Our aim is now to determine the seal displacement response $z(t, \xi)$ to a fluid pressure signal $p(t, \xi)$.

If the system is linear, the following convolution integral holds :

$$p(t, \xi) = \int_{-\infty}^{\infty} h(t-\tau, \xi) \cdot x(\tau, \xi) \cdot d\tau \quad (8.1)$$

The impulse response function $h(t, \xi)$ describes the system stress response to a Dirac-pulse displacement input in the time domain. The transfer function $H(f, \xi)$ was determined in the frequency domain using a dynamic FEM analysis of the seal. When $H(f, \xi)$ is known the compliance function $G(f, \xi)$ in the frequency domain can be expressed as

$$G(f, \xi) = 1/H(f, \xi) \quad (8.2)$$

The compliance function $g(t, \xi)$ in the time domain can be derived from $G(f, \xi)$ by an inverse Fourier transform, where

$$g(t, \xi) = F^{-1}\{G(f, \xi)\} = \int_{-\infty}^{\infty} G(f, \xi) \cdot \exp(j2\pi ft) \cdot df \quad (8.3)$$

The compliance function $g(t, \xi)$ can then be used to calculate the seal displacement response $z(t, \xi)$ due to the fluid film pressure signal $p(t, \xi)$ using :

$$z(t, \xi) = \int_{-\infty}^{\infty} g(t-\tau, \xi) \cdot p(\tau, \xi) \cdot d\tau \quad (8.4)$$

Note that H and G are complex, whereas h, g, p, x and z are real.

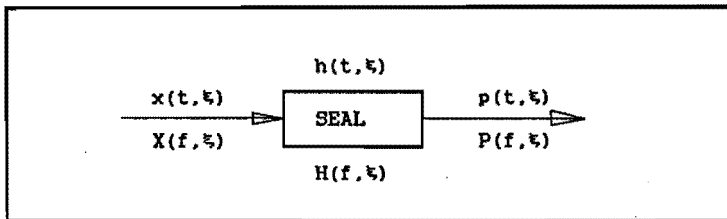


Fig 8.2 : Block diagram representing the input displacement signal, the seal transfer function and the pressure response signal.

8.4 FEM MODEL OF THE SEAL.

A virgin standard Nitrile rubber radial lip seal was modeled using the MARC FEM software (version K2), see [5]. The seal-shaft contact

problem was assumed to be axisymmetric and isothermal ($T=30\text{ }^{\circ}\text{C}$). The FEM model consists of 355 hybrid, bi-linear displacement, constant pressure, quadrilateral axisymmetric ring elements [5], see Figure 8.3. The garter spring was modeled using 1 spring element connected to the seal by 6 rigid beam elements. The beam elements restrain the displacements but not the rotations and provide a pinned rigid link between the nodes on the seal and a node on the end of the spring element. A distinction is made between (a) a static deformation component x_s corresponding to the interference fit between the shaft diameter and the undeformed seal diameter, and (b) a small-amplitude sinusoidal deformation component $x_d(t)$, which is superimposed on x_s . Both $x_d(t)$ and x_s do not vary with ξ . The static deformation results in a static contact stress component $p_s(\xi)$, see also chapter 3. The sinusoidal deformation results in a dynamic stress component $p_d(t, \xi)$. Thus for the total radial displacement $x_t(t)$ holds :

$$x_t(t) = x_s + x_d(t) = x_s + |x_d| \cdot \cos(\omega \cdot t) \quad (8.5a)$$

It is assumed that the total contact stress $p_t(t, \xi)$ can be written as

$$p_t(t, \xi) = p_s(\xi) + p_d(t, \xi) = p_s(\xi) + |p_d(\xi)| \cdot \cos(\omega \cdot t + \phi) \quad (8.5b)$$

The static component $p_s(\xi)$ was calculated using the Mooney-Rivlin material model, [7]. In this model the homogeneous, isotropic nonlinear mechanical behaviour of the seal rubber is described by 2 constants, C_1 and C_2 . The static component $p_s(\xi)$ was calculated taking into account the physical and geometrical nonlinearities of the seal-shaft contact problem (see also chapter 3). Thus note that the relation between p_s and x_s is nonlinear. Because the amplitude of the sinusoidal excitation is small, it is assumed that the material behaviour under dynamic load can be linearized. In [8] Morman and Nagtegaal present a general method for the analysis of incompressible viscoelastic material solids, in which a small-amplitude harmonic oscillation is superimposed on a static deformation field. The material behaviour is assumed to be of the "fading memory" type describable by linear viscoelastic theory. "Fading memory" indicates that under constant deformation, the resulting stress will eventually relax to equilibrium values that depend only on the maintained strain. The method from [8] as implemented in the nonlinear FEM program MARC was used here to calculate the dynamic seal response. To determine the linear viscoelastic response to a sinusoidal small-amplitude excitation, phi-coefficients had to be derived from the stress relaxation function $G(t)$, see [8]. C_1 , C_2 and $G(t)$ have been determined by curve-fits on experimental data from uni-axial stress-relaxation tests performed on a Nitrile rubber specimen at constant temperature of $T=30\text{ }^{\circ}\text{C}$, defining $G(t)$ as:

$$G(t) = G_0 + \sum_{i=1}^7 G_i \cdot \exp(-t/\tau_i) \quad (8.6)$$

Apart from visco-elastic effects the FEM model also takes into account both the inertia of the lumped garter spring mass and the inertia of the continuously distributed Nitrile rubber mass. A list of the physical properties used in the FEM model is given in appendix A3.

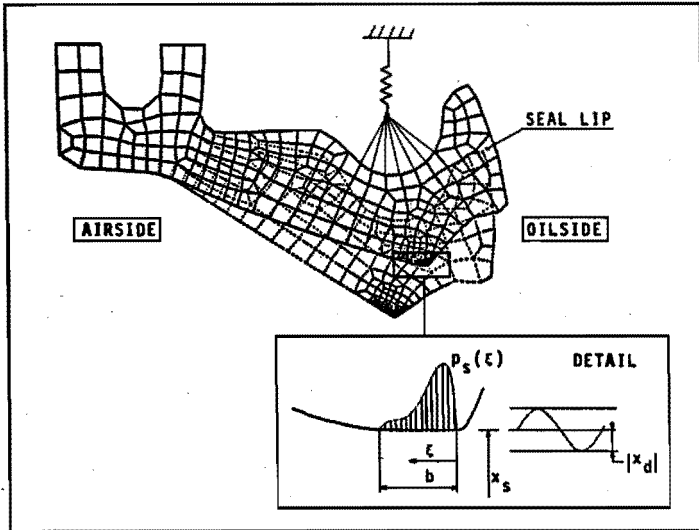


Fig 8.3 : FEM model of the seal.

8.5 TRANSFER FUNCTION OF THE SEAL.

First a static deformation $x_s = 1.01$ mm was applied to the seal, corresponding to the mounting position of the seal on an imaginary shaft with radius $R+e$, where R is the nominal radius of the actual shaft and e is the eccentricity (see fig 8.5). Next a sinusoidal radial displacement signal $x_d(t, \xi) = |x_d| \cdot \cos(2\pi ft)$, $|x_d| = 0.01$ mm, was applied simultaneously to all of the 10 nodes in the contact area (contact width $b = 75$ μm).

For each node i ($i=1, 2, \dots, 10$) in the contact area a linearized transfer function $H(f, \xi_i)$ was defined:

$$H(f, \xi_1) = \frac{P(f, \xi_1)}{X(f, \xi_1)} = \frac{P(f, \xi_1)}{X(f)} \quad (8.7)$$

Where $P(f, \xi_1)$ is a complex variable representing the Fourier transform of $p_t(t, \xi_1)$ at node i , and $X(f)$ represents the Fourier transform of $x_t(t)$. $H(f, \xi_1)$ was linearized around $x_s(\xi_1) = x_s = 1.01$ mm.

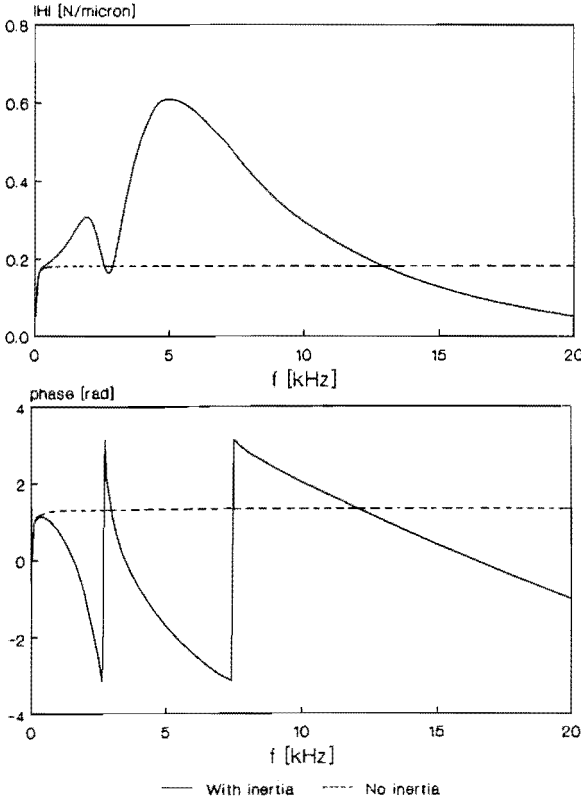


Fig 8.4 : The amplitude of the transfer function of the seal $|H(f, \xi_3)|$ and phase shift angle $\phi(f, \xi_3)$.

At node $i=3$ ($\xi_3 = 18 \mu\text{m}$) the maximum of the static contact stress $p_s(\xi)$ occurs ($p_s(\xi_3) = 4.7$ MPa). It is therefore expected that in case of separation of seal and shaft surface, node $i=3$ will be the last to remain in contact with the seal (separation under dynamic excitation could not be modeled using the K2 version of MARC).

Figure 8.4 shows the amplitude of the transfer function $|H(f, \xi_1)|$ for $i=3$. Note the effect of the seal and spring inertia: below $f=100$ Hz the two solutions for $|H(f, \xi_3)|$ merge, whereas at higher frequencies

differences occur in amplitude and phase-shift. Assuming that the seal separates as soon as $p_t(t, \xi_3)$ becomes negative, thus when :

$$p_s(\xi_3) + p_d(t, \xi_3) < 0, \quad (8.8)$$

it was found that for $|x_d| = 10 \mu\text{m}$ loss of contact already occurs for $f > 1.8 \text{ Hz}$. As in practice the vibration input signal will contain low-amplitude high-frequency components, it is necessary to include seal and spring inertia in the model. These components may originate from vibrations induced by roller bearings, gear trains, engines, or from shaft eigenfrequencies, etc.

8.6 INTERACTION BETWEEN FLUID FILM AND VISCOELASTIC SEAL.

In this paragraph the interaction between the viscoelastic, inertial seal behaviour and the fluid film is investigated in case of a whirling shaft. Only steady-state conditions are considered. It is assumed that the shaft surface is a perfect smooth cylinder, and that the shaft center C_{sh} rotates around the seal center C_{se} at whirl angular velocity ω_w as represented in fig 8.5. Fully flooded conditions are assumed in the clearances.

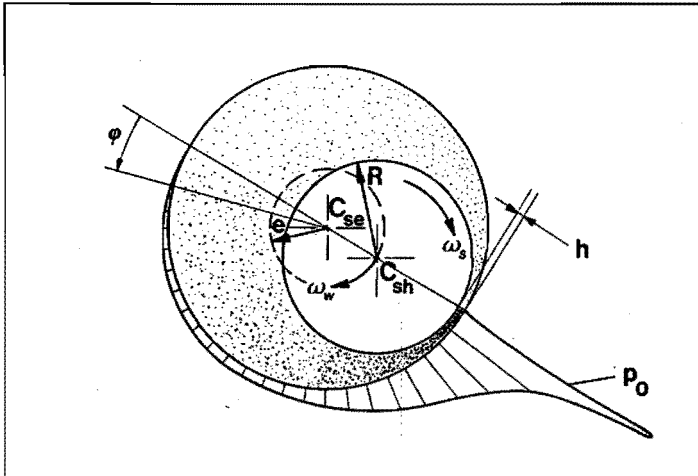


Fig 8.5 : Fluid film geometry and pressure distribution of a whirling shaft in a rigid bearing.

If the whirling frequency f_w (where $f_w = 2\pi\omega_w$) of the shaft is sufficiently high, the seal will be forced to perform oscillations around a stretched state (at radius $R+e$), because its inertial and viscous behaviour and the fluid film pressure will impede the rebound of the seal.

The relationship between the fluid film pressure and the film geometry is given by Reynolds' equation, for Newtonian fluids. If the shaft and seal centre line are parallel, this equation reads, in cylindrical coordinates :

$$\frac{1}{R^2} \frac{\partial}{\partial \theta} \left(h^3 \frac{\partial p}{\partial \theta} \right) + \frac{1}{b^2} \frac{\partial}{\partial \zeta} \left(h^3 \frac{\partial p}{\partial \zeta} \right) = \frac{1}{2} (\omega_s + \omega_{se}) \frac{\partial h}{\partial \theta} + \frac{\partial h}{\partial t} \quad (8.9a)$$

where : θ is a circumferential coordinate.
 $\zeta = \xi/b$ is a nondimensional axial coordinate.
 ω_s is the shaft angular velocity.
 ω_{se} is the seal angular velocity.

For a radial lip seal b/R is of the order of 10^{-3} , hence a short bearing model will be used, neglecting the pressure induced flow in circumferential direction with respect to the shear induced flow in circumferential direction, see [13] :

$$\frac{\partial}{\partial \xi} \left(h^3 \frac{\partial p_0}{\partial \xi} \right) = \frac{1}{2} (\omega_s + \omega_{se}) \frac{\partial h}{\partial \theta} + \frac{\partial h}{\partial t} \quad (8.9b)$$

where the subscript 0 denotes the short bearing approximation.

Because the Reynolds equation does not incorporate fluid inertia effects, it is invariant to the choice of the frame of reference. Upon the introduction of a rotating reference system (see e.g. Booker [10] or Childs et al. [11]) (8.9b) can be simplified considerably. Two convenient choices for the (arbitrary) angular velocity of this reference system are (a) $\omega = \omega_w$, yielding a stationary bearing problem with entrainment effects only, or (b) $\omega = \omega_s/2$, resulting in a dynamically loaded bearing problem with squeeze effects only. Both cases produce the same pressure distribution (and film thickness profile). The pressure distribution p_0 can now be expressed by (case (a)) :

$$\frac{\partial}{\partial \xi} \left(h^3 \frac{\partial p_0}{\partial \xi} \right) = \frac{1}{2} (\omega_s + \omega_{se} - 2\omega_w) \frac{dh}{d\phi}$$

where $\phi = \theta + \omega_w \cdot t$

Or, using $\omega_{se} = 0$:

$$\frac{\partial}{\partial \xi} \left(h^3 \frac{\partial p_0}{\partial \xi} \right) = -(\omega_w - \omega_s/2) \frac{dh}{d\phi} \quad (8.9c)$$

If it is assumed that $p_0(\phi, \xi=0) = p_0(\phi, \xi=b)=0$, then (8.9c) is easily integrated to obtain :

$$p_0(\phi, \xi) - A \cdot \frac{dh}{h^3} = 0 \quad (8.9d)$$

$$\text{where } A = -6\eta b^2(\omega_w - \omega_s/2) \frac{\xi}{b} \left(\frac{\xi}{b} - 1 \right) \quad (8.9e)$$

Cavitation is simulated by setting $p_0 = p_{cav}$ where $p_0 \leq p_{cav}$. It was assumed that (8.9d) is only valid outside the cavitation region.

This pressure distribution p_0 rotates along the seal surface at frequency f_w . A material point at $\xi = \xi_3$ in the contact area experiences the time dependent pressure according to equation (8.9e), where $\phi = 2\pi \cdot f_w \cdot t$. Now the pressure signal equals $p(t, \xi_3) = p_0(t, \xi_3) - p_s(\xi_3)$. Here $p_s(\xi_3)$ represents the static contact stress for a seal stretched at a radius $R+e$.

The viscoelastic displacement response $z(t, \xi_3)$ of the seal, due to $p(t, \xi_3)$ will now be studied. Assuming that both z and p are periodic with period time $T=1/f_w$, equation (8.4) can be expressed as :

$$z(t, \xi) = z(t+nT, \xi) = \int_0^T g(t-\tau, \xi) \cdot p(\tau, \xi) \cdot d\tau \quad (8.10)$$

The total film thickness $h(t, \xi_3)$ can now be written as :

$$\begin{aligned} h(t, \xi_3) &= h(t+nT, \xi_3) = h_1(t) + z(t, \xi_3) \\ &= e \cdot (1 + \cos(2\pi f_w t)) + z(t, \xi_3) \end{aligned} \quad (8.11)$$

where h_1 represents the gap height for a seal stretched at radius $R+e$. Now that the relation between pressure and film thickness is defined, the differential equation (8.9) can be solved numerically via (a) a direct method, or (b) an implicit method. Both numerical iteration schemes can be employed using either the classical EHD formulation (considering $p=p(h)$) or the inverse EHD formulation (considering $h=h(p)$). The implicit method in combination with the classical EHD formulation showed the best convergence.

Because of the large differences in magnitudes of p and h equation (8.9d) was scaled numerically. Therefore we write :

$$p = \hat{p} \cdot \bar{p} \quad ; \quad h = \hat{h} \cdot \bar{h} \quad ; \quad \frac{dh}{d\phi} = \hat{h} \cdot \frac{d\bar{h}}{d\phi} \quad ; \quad h_1 = \hat{h} \cdot \bar{h}_1$$

and for equation (8.9d) :

$$\bar{p} \cdot \bar{h}^3 + A^* \cdot \frac{d\bar{h}}{d\phi} = 0 \quad (8.12)$$

Here we have used $\hat{p} = 10^6$, $\hat{h} = 10^{-6}$ and $A^* = A \cdot 10^6$
 For (8.12) we write in discrete form the following system of N nonlinear equations

$$f_i = \bar{p}_i \cdot \bar{h}_i^3 + A^* \cdot \left(\frac{d\bar{h}}{d\phi}\right)_i = 0 \quad (i=0,1,\dots,N-1) \quad (8.13)$$

where $\bar{h}_i = \bar{h}_{1i} + \sum_{j=0}^{N-1} \bar{g}_{i-j} \cdot \bar{p}_j$ (8.14)

Here $\left(\frac{d\bar{h}}{d\phi}\right)_i$ was calculated via a second order backward difference scheme.

The set of nonlinear equations $f_i(p_0, p_1, \dots, p_{N-1}) = 0$ of equation (8.13) was solved using a Newton-Raphson iteration scheme. The Jacobian was approximated by first order forward differences and was updated each iteration step. The Jacobian A is not banded but a full matrix. To solve the set of linear equations $Ax=b$ in the Newton Raphson scheme an accurate solver was used, taking into account corrections based on the residual vector, see [12].

8.7 DISCUSSION.

Appendix A3 contains a list of parameter values used for the calculations. In the frequency range $(f_w - f_s/2) > 5$ Hz a full lubrication film was only found for $p_s \leq 0.2$ MPa, whereas for a virgin seal $p_s(\xi_3) = 4.7$ MPa. For $p_s > 0.2$ MPa no solution was found. This could be explained as follows :

- 1) For a virgin seal a full film lubrication is physically not possible when $p_s(\xi_3) > 0.2$ MPa
- 2) Fluid inertia should be taken into account.
- 3) Microasperity lubrication may not be neglected.

ad 1) : In practice the seal torque and the seal wear rate are high during a run-in period of a virgin seal. After this run-in period the torque is considerably lower and the seal wear rate reduces to almost zero. This could be interpreted as a transition from mixed lubrication to full film lubrication, thus confirming the assumption that for a virgin seal full film lubrication is not possible.

Dynamic FEM calculations on worn (run-in) seal geometries have a limited value only, as long as the changes in the mechanical properties of the rubber in the contact area due to additional vulcanisation, physical and chemical ageing, and oil absorption during running in can not be taken into account.

ad 2) The lubrication model does not take into account fluid inertia. As the maximum value of the local Reynolds number

$Re = \frac{\rho \omega R h}{\eta} \approx 1, < 500$, fluid inertia will only yield a minor increase in load carrying capacity, see [14].

ad 3) Microasperity lubrication due to surface asperities will also contribute to the load carrying capacity of the lubricating film.

In order to illustrate the macro lubrication principle the results calculated for $p_s(\xi_3) = 0.2$ MPa will be used.

Figure 8.6 shows one period of the pressure signal $p_0(t, \xi_3)$ for different whirling frequencies f_w , where $f_w = f_s$. Note the occurrence of cavitation ($p_{cav} = -10$ kPa), resulting in a positive load carrying capacity.

Figure 8.7 shows a plot of the total film thickness $h = h(t, \xi_3)$ corresponding to the pressure signals from fig. 8.6.

Note that at lower frequencies the seal rebound is stronger resulting in a lower average film height.

Because the viscoelastic (and the inertial) seal response is essential in this macro lubrication mechanism, this type of lubrication may be called visco-elastohydrodynamic (VEHD) lubrication. The author believes that this VEHD lubrication concept plays an important role in the lubrication mechanism of radial lip seals.

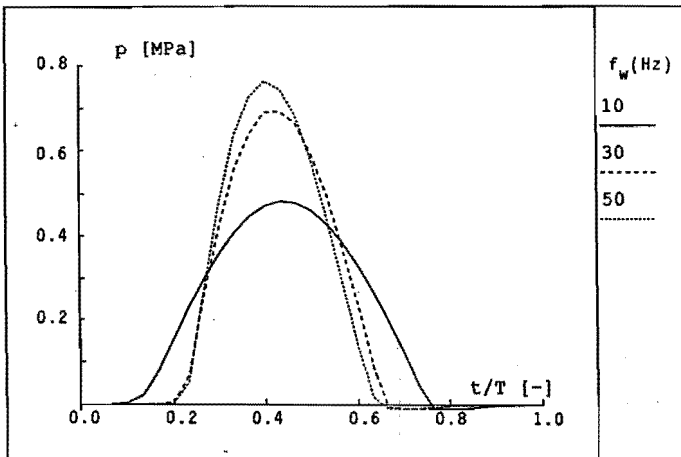


Fig 8.6 : Pressure signal $p_0(t, \xi_3)$, for different values of the whirl frequency f_w , where $f_w = f_s$

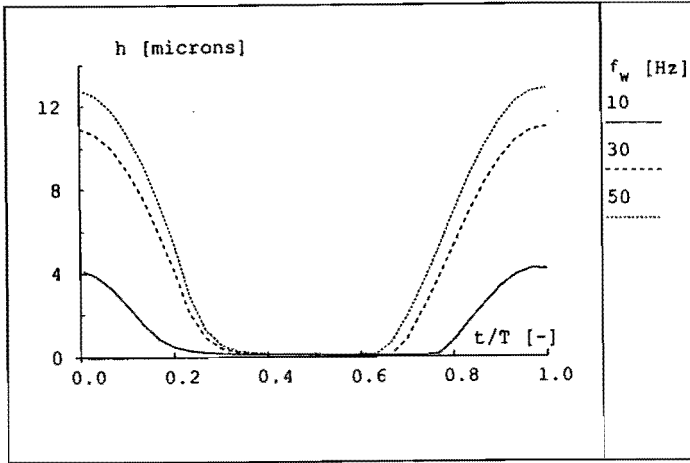


Fig 8.7 : Total film thickness $h=h(t, \xi_3)$, corresponding to the pressure signal from fig 8.6.

8.8 CONCLUSIONS.

- 1) It is not allowed to assume a steady deformation state in the lip, because a dynamic excitation of the seal lip will occur due to out of roundness of the shaft or radial motions of the shaft center.
- 2) Even for very low amplitude shaft vibrations the seal separates from the shaft at relatively low oscillation frequencies.
- 3) This separation introduces fluid filled clearances.
- 4) Visco-elastohydrodynamic lubrication can create a positive load carrying capacity.

8.9 REFERENCES.

- [1] Hirano, F., and Ishiwata, H. The lubricating condition of a lip seal, Proc.Instn.Mech.Engrs., Vol. 180, Pt. 3B, 1965-66, Paper 15, pp.187-196.
- [2] Jagger, E.T. Rotary shaft seals: the sealing mechanism of synthetic rubber seals running at atmospheric pressure, Proc.Instn.Mech.Engrs., Vol.171, No.18, 1956-57, pp.597-616 (Note: see especially the discussion).

- [3] Prati, E. A theoretical-experimental method for analyzing the dynamic behaviour of elastomeric lip seals .Rubber Chemistry & Technology, Vol. 60, No. 1., 1987, pp 176-189.
- [4] Gawlinski, M. and Konderla, P. Dynamic analysis of oil lip seal , Proc. 10th International Conference on fluid sealing, Innsbruck, Austria, April 3-5,1984 , paper C4, ppl39-155.
- [5] MARC Analysis Research Corporation, Palo Alto, California, U.S.A., FEM software, User manuals, version K2, 1986.
- [6] ten Hagen, E.A.M. Mechanische karakterisering van afdichtingsrubbers., M.Sc. Thesis, Eindhoven University of Technology, Jan. 1988.(in Dutch)
- [7] Treolar, L.R.G. The physics of rubber elasticity, Clarendon Press, Oxford, 1975.
- [8] Morman, K.N. Jr., and Nagtegaal, J.C. Finite element analysis of sinusoidal small amplitude vibrations in deformed viscoelastic solids, Int. J. Num. Meth. Eng., Vol.19, No.7, 1983, pp 1079-1103
- [9] Mueller, H.K. Concepts of sealing mechanism of rubber lip type rotary shaft seals. Proc. 11th Conf. on Fluid Sealing BHRA, 1987,paper K1, pp 698-709.
- [10] Booker, J.F. Dynamically Loaded Journal Bearings: Mobility Method of Solution, Journal of Basic Engineering, Trans. ASME, Series D, Vol.87, No.3, Sept. 1965, pp. 537-546.
- [11] Childs,D., Moes, H. and van Leeuwen, H. Journal Bearing Impedance Descriptions for Rotordynamic Applications, Journal of Lubrication Technology, Trans. ASME, Series F, Vol.99, No.2, April 1977, pp. 198-214.
- [12] NAG fotran library manual Mark 8, 1980.
NAG Central Office, Oxford, England.
- [13] Du Bois, G.B., Ocavirk, F.W. Analytical derivation and experimental evaluation of short-bearing approximation for full journal bearings. NACA report No. 1157, 1954.
- [14] Raimondi, A.A and Szeri, A.Z. Journal and thrust bearings. in : Handbook of lubrication, Vol 2, by Rooser, E.R. (ed.), CRC press Inc, Boca Raton, Florida, 1984, pp 417-420.

CHAPTER 9 : FINAL REMARKS.

9.0 OVERVIEW.

9.1 Practical utility of this study.

9.2 Main conclusions.

9.3 Future research.

In this final chapter the practical utility of this study is evaluated. The main conclusions are summarized and at the end recommendations for future research are given.

9.1 PRACTICAL UTILITY OF THIS STUDY.

The general objective of this study was to get a better insight into the sealing mechanism and lubrication mechanism of radial lip seals. A better insight is necessary in order to come to a more optimal seal design.

In contrast with most of the literature on radial lip seals, the accent of this thesis is not on the analysis of experimental results. Concentrating on experiments to investigate the functioning of radial lip seals can lead to erroneous interpretation of the results, with the current state of insight into the basic physical principles.

In this thesis attempts are made to study the sealing and lubrication mechanisms with an accent on developing theoretical models. A hazardous aspect of developing theoretical models in seal research is that, due to the complexity of the physical reality, these models are based on numerous assumptions and simplifications.

The practical usefulness of the thermal network model approach in chapter 5 to calculate the seal-shaft contact temperatures is illustrated by the good correspondence between measurements and calculations.

The pumping, the leakage and the lubrication model presented in chapters 6, 7 and 8 of this thesis do give a better insight into the principles of the sealing and lubrication mechanism, but the practical use of these models for the seal designer and seal application engineer are still limited at present. However, in seal research these models can be used to come to a better defined experimental approach. In the near future, a combination of detailed theoretical models and well-defined experiments will lead to designing rules for a more optimal seal.

It is the hope of the author that through this study a small new contribution is made to the over 30 year old discussion on the basics of radial lip seals.

9.2 MAIN CONCLUSIONS.

The main conclusions of this thesis are summarized as follows

- 1) The sealing mechanism is based on an active pumping action of the seal.
- 2) The pumping mechanism of radial lip seals is counterbalanced by the capillary suction forces of the oil-air interface on the air-side of the seal.
- 3) The capillary forces play an important role in the lubrication mechanism. Without these capillary suction forces starved lubrication would occur.
- 4) Above a certain angular velocity cavitation occurs in the contact area, starting on the edges of the contact zone.
- 5) The seal pumping action can be explained on basis of a visco-seal concept.
- 6) Seal leakage at higher angular velocities can be explained on basis of a breakdown of the oil-air interface on the airside of the seal due to centrifugal forces on the oil.
- 7) Studying the sealing and lubrication mechanism of radial lip seals, the static analysis of the seal-shaft contact conditions has only a limited value because the contact conditions are strongly influenced by the dynamic effects of out of roundness or eccentricity of the shaft.
- 8) Visco-elastohydrodynamic (VEHD) lubrication can play an important role in the lubrication mechanism of radial lip seals.

9.3 FUTURE RESEARCH.

Future research on seals should concentrate on an experimental investigation of the seal under dynamic conditions, e.g. by vibration analysis. Due to the nonlinearity of the dynamic seal-shaft contact it is advisable to perform vibration measurements based upon time-domain

techniques. The linearisation in the frequency domain e.g. by using Fast Fourier Transform (FFT) techniques could introduce problems concerning the limited levels of excitation.

To measure the contact behaviour under dynamic conditions there is a strong need for high-speed low-pressure pressure transducers in order to validate the numerical FEM results of the contact stresses.

The generally used method of characterizing rubber under (quasi-) static conditions has only a limited practical value, because in practice seals operate under dynamic conditions. Therefore more attention should be paid to an accurate experimental and theoretical characterisation of the nonlinear thermo-viscoelastic rubber material behaviour under dynamic conditions.

As mentioned in chapter 6, the active pumping mechanism is probably based on a number of mechanisms, acting simultaneously. A detailed study is necessary into the interaction of the 'visco-seal', the 'reciprocating motion' and the 'cascade' pumping mechanism under dynamic conditions.

There is also a need for a detailed theoretical and experimental study on the micro and macro lubrication mechanisms. It would be interesting to incorporate microasperity lubrication effects of seal and shaft roughness into the macro-VEHD lubrication model.

APPENDIX A1 : CALCULATION OF THE PRESSURE DROP OVER THE OIL-AIR INTERFACE.

The formation of an oil-air interface and the occurrence of a pressure drop Δp over an oil-air interface can be physically explained in terms of minimization of the system energy. For the physical backgrounds the reader is referred to [5] of chapter 2.

In this appendix we will confine ourselves to calculating the pressure drop Δp over the oil-air interface on the airside of the seal when the location of the oil-air interface, i.e. the x-coordinate of the oil-air interface is known, see figure A1.1.

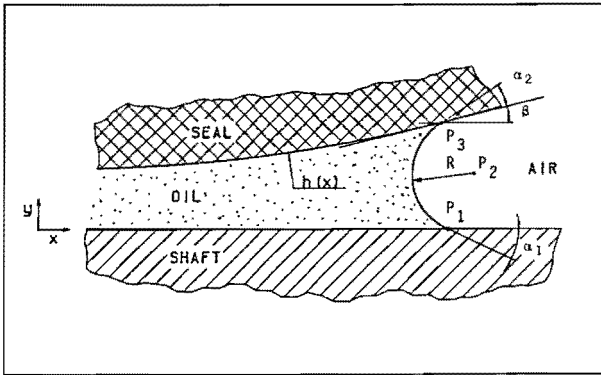


Fig. A1.1 : Oil-air interface.

The following assumptions and simplifications are made :

- 1) In the x-y plane, the oil-air interface has a constant curvature $1/R_{xy} = 1/R$. The curvature $1/R_{xz}$ in the xz-plane is small and can be neglected compared to $1/R_{xy}$.
- 2) The influence of temperature on γ , α_1 and α_2 is neglected.
- 3) The influence of velocity on γ , α_1 and α_2 is neglected.
- 4) The influence of centrifugal forces and gravity forces on the curvature R of the oil-air interface is neglected.

Based on these assumptions the calculation of Δp is relatively simple. For the coordinates (x_2, y_2) of the center point P_2 of the oil-air interface we can write:

$$x_2 = x_1 + R \cdot \sin \alpha_1 \quad (A1.1)$$

$$y_2 = R \cdot \cos \alpha_1 \quad (A1.2)$$

where x_1 is the x-coordinate of point P_1 .

For the coordinates (x_3, y_3) of point P_3 , where the oil-air interface is in contact with the seal surface we write, using equation (A1.1) and (A1.2):

$$x_3 = x_2 - R \cdot \cos\psi = x_1 + R \cdot (\sin\alpha_1 - \cos\psi) \quad (\text{A1.3})$$

$$y_3 = y_2 + R \cdot \sin\psi = R \cdot (\cos\alpha_1 + \sin\psi) \quad (\text{A1.4})$$

where $\psi = \frac{\pi}{2} - (\alpha_2 + \beta)$ (A1.5)

$$\beta = \arctan \left. \frac{dh}{dx} \right|_{x_3} \quad (\text{A1.6})$$

Using equation (A1.4) we now write:

$$h(x_3) = y_3 = R \cdot (\cos\alpha_1 + \sin\psi) \quad (\text{A1.7})$$

or,

$$h(x_3) = R(x_1) \cdot (\cos\alpha_1 + \sin(\alpha_2 + \arctan \left. \frac{dh}{dx} \right|_{x_3})) \quad (\text{A1.8a})$$

where $x_3 = x_1 + R(x_1) \cdot (\sin\alpha_1 - \sin(\alpha_2 + \arctan \left. \frac{dh}{dx} \right|_{x_3}))$ (A1.8b)

For a certain value x_1 , the radius $R = R(x_1)$ of the oil-air interface can now be determined from equation (A1.8a) and (A1.8b) using a numerical root finding algorithm, e.g. a Newton-Raphson scheme. The pressure drop $\Delta p(x_1)$ can now be calculated using

$$\Delta p(x_1) = \gamma \left(\frac{1}{R_{xy}} + \frac{1}{R_{xz}} \right) \approx \frac{\gamma}{R_{xy}} = \frac{\gamma}{R(x_1)} \quad (\text{A1.9})$$

The wetting angles α_1 and α_2 can be determined by measuring the contact angle of a droplet of oil on a flat surface of rubber respectively steel. An accurate experimental determination of α_1 and α_2 however, is difficult due to hysteresis effects, the influence of surface roughness, and the influence of gravity forces. Measuring α_2 we have an extra complication: due to diffusion of oil into the rubber the wetting angle α_2 can change within 30 minutes from 15 to 30 degrees.

The data represented in figures 2.4 and 2.6 were calculated using the following values :

$$\begin{aligned} \alpha_1 &= 0.122 \text{ rad (7.0 degr.)} \\ \alpha_2 &= 0.524 \text{ rad (30.0 degr.)} \\ \gamma &= 0.0315 \text{ N/m} \end{aligned}$$

The experiments have been performed using Shell oil Tellus 46.

APPENDIX A2: A LEAKAGE MODEL FOR RADIAL LIP SEALS.

INTRODUCTION.

In this appendix a model is derived which describes seal leakage as a result of a breakdown of the oil-air interface on the airside of the seal, resulting from centrifugal forces acting on the oil. It is assumed that the pressure distribution across the clearance can become so high, that the surface tension is no longer able to prevent a breakdown of the interface. Two different cases are studied. For case 1 the seal is fixed, and the shaft is rotating. For case 2 the shaft is fixed, and the seal is rotating.

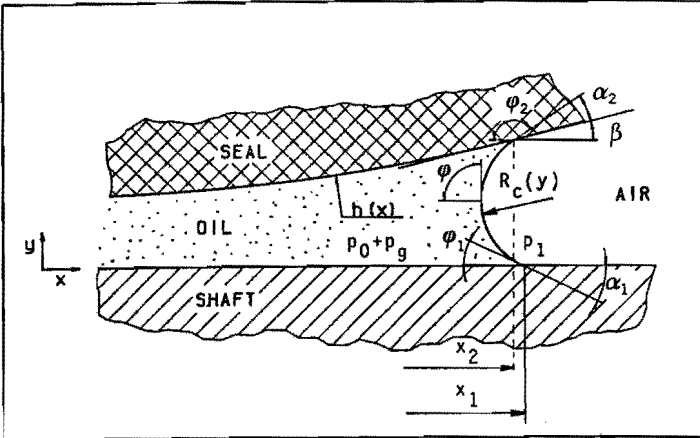


Fig A2.1 : Meniscus on airside of the seal.

CASE 1 : $\omega_1 \neq 0$; $\omega_2 = 0$.

Assuming a laminar Couette flow in the clearance on the airside of the seal we write for the velocity u in circumferential direction :

$$u = \frac{\omega R}{h}(h-y) \quad (A2.1)$$

where $h = h(x_1)$ and R represents the radius of the shaft.

At the oil-air interface the equilibrium of pressure gives :

$$P_0 + P_c(y) + \sigma \left(\frac{1}{R_c(y)} + \frac{1}{R_z(y)} \right) + P_g = P_1 \quad (\text{A2.2})$$

where P_0 = pressure in machine.

P_c = pressure due to centrifugal forces.

P_g = pressure due to gravity forces.

P_1 = ambient pressure.

R_c = principal radius of the curvature of the interface.

R_z = principal radius connected with the ring shape of the interface.

Because $\frac{1}{R_c} \gg \frac{1}{R_z}$, the term $\frac{1}{R_z}$ will be neglected from now on.

From the Navier-Stokes equations it follows that the relation between the pressure in the oil film and the centrifugal forces is :

$$\frac{dp_c}{dy} = \frac{\rho u^2}{(R+y)} \approx \frac{\rho u^2}{R} \quad \text{when } y \ll R \quad (\text{A2.3})$$

The function $R_c(y)$ and the function $\phi(y)$ describing the shape of the interface are related by :

$$\frac{1}{R_c} = \frac{d\phi}{dy} \cdot \sin\phi \quad (\text{A2.4})$$

Equation (A2.1) with (A2.3) gives :

$$\begin{aligned} P_c(y) &= \int_0^y \rho \frac{u^2}{R} dy = \frac{\rho \omega^2 R^2}{3h^2 R} (h^3 - (h-y)^3) \\ &= -\frac{\rho \omega^2 R}{3 h^2} (h-y)^3 + P_c(y=h) \end{aligned} \quad (\text{A2.5})$$

Equation (A2.2) with (A2.4) gives :

$$P_1 - P_0 - P_g - P_c(y) = \frac{\sigma}{R_c(y)} = \sigma \sin\phi \frac{d\phi}{dy} \quad (\text{A2.6})$$

For the hydrostatic oil pressure due to gravity forces (see fig. A2.2) we write:

$$P_g = (h_0 + R(1 - \sin\theta)) \rho g \quad \text{for } h_0 > -2R \quad (\text{A2.7})$$

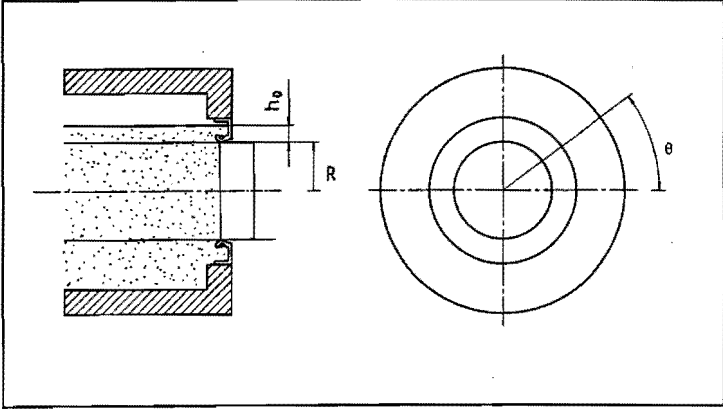


Fig A2.2 : Definition of the oil level h_0 and angular coordinate θ .

Integrating (A2.6) gives :

$$\int_0^y \left(\frac{P_1 - P_0 - P_g}{\sigma} + \frac{\rho \omega^2 R}{3\sigma h^2} (h-y)^3 - \frac{P_c(h)}{\sigma} \right) dy = \int_{\phi_1}^{\phi} \sin\phi d\phi \quad (A2.8)$$

Substituting $y=h$ in (A2.8) gives :

$$P_c(h) = \sigma \frac{\cos\phi_2}{h} - \sigma \frac{\cos\phi_1}{h} + P_1 - P_0 - P_g + \frac{\rho \omega^2 R h}{12} \quad (A2.9)$$

where $\phi_1 = \alpha_1$

$$\phi_2 = \pi - (\alpha_2 - \beta) ; \beta = \arctan\left(\frac{dh}{dx}\bigg|_{x_2}\right) - \arctan\left(\frac{dh}{dx}\bigg|_{x_1}\right)$$

Substituting $y=y$ in (A2.8) gives :

$$\frac{P_1 - P_0 - P_g}{\sigma} y - \frac{\rho \omega^2 R}{\sigma h^2} (h-y)^4 + \frac{\rho \omega^2 R h^2}{12\sigma} - \frac{P_c(h)}{\sigma} y = -\cos\phi + \cos\phi_1 \quad (A2.10)$$

Using (A2.9) and (A2.10) gives :

$$\cos\phi = \cos\phi_1 \left(1 - \frac{y}{h}\right) + \cos\phi_2 \left(\frac{y}{h}\right) + \frac{\rho \omega^2 R}{12\sigma h^2} \left\{ (h-y)^4 - h^4 + h^3 y \right\} \quad (A2.11)$$

Differentiating (A2.11) gives :

$$\sin\phi \frac{d\phi}{dy} = \frac{\cos\phi_1}{h} - \frac{\cos\phi_2}{h} - \frac{\rho \omega^2 R}{12\sigma h^2} \left\{ -4(h-y)^3 - h^3 \right\} \quad (A2.12)$$

Note that when $\frac{d\phi}{dy} = 0$ the radius of the curvature goes to infinity by virtue of (A2.4). For $\frac{d\phi}{dy} < 0$ the interface can no longer be closed across the clearance, a breakdown of the interface then occurs, and therefore leakage will take place. No breakdown will occur as long as the left-hand side of (A2.12) is positive for all y , thus as long as

$$\cos\phi_1 - \cos\phi_2 > \frac{\rho \omega^2 R h^2}{12 \sigma} \quad (\text{A2.13})$$

This sealing criterion was also formulated by Bootsma [7.2], in terms of a Weber number We , where

$$We = \frac{\rho \omega^2 R h^2}{\sigma}$$

The sealing criterion formulated by Bootsma does not depend on the value of the pumping pressure Δp (where $\Delta p = p_1 - p_0 - p_g$), because he assumed a plain section with a constant clearance h .

Taking into account the curved section of the seal lip where $h=h(x)$ we find that the leakage criterion formulated in equation (A2.13) becomes a function of the seal pumping pressure Δp (as illustrated in figure 7.3 of chapter 7).

Our aim is now to determine the location and the shape of the interface taking into account centrifugal forces.

Using (A2.2), (A2.4) and (A2.12), and then substituting $y=0$ it can be shown that :

$$p_1 - p_0 - p_g - \frac{\sigma \cos\phi_1}{h} - \frac{\sigma \cos\phi_2}{h} - \frac{\rho \omega^2 R h}{4} = 0 \quad (\text{A2.13})$$

Substituting (A2.7) and $h=h(x_1)$ in (A2.13) gives :

$$p_1 - p_0 - (h_0 + R(1 - \sin\theta))\rho g - \frac{\sigma \cos\phi_1}{h(x_1)} - \frac{\sigma \cos\phi_2}{h(x_1)} - \frac{\rho \omega^2 R h(x_1)}{4} = 0 \quad (\text{A2.14})$$

Also the following equation holds :

$$x_1 + \int_0^{h(x_2)} \cos\phi \cdot (1 - \cos^2\phi) dy - x_2 = 0 \quad (\text{A2.15})$$

The coordinates x_1 and x_2 can now be obtained by solving the system of non-linear equations (A2.14) and (A2.15) when the function $h(x)$ is known.

The function $h(x)$ was determined from the deformed geometry of the finite element calculations (see chapter 3). The equations (A2.14) and (A2.15) have been solved numerically using a Newton-Raphson iteration scheme (see chapter 7 for the results).

CASE 2 : $\omega_1 = 0$; $\omega_2 \neq 0$.

Assuming a laminar Couette flow in the clearance on the airside of the seal we now write for the velocity u in circumferential direction :

$$u = \frac{\omega R}{h} y \quad (\text{A2.15})$$

where $h = h(x_1)$

In analogy with the theory derived for case 1 we now find the rotating seal will not leak as long as

$$\cos\phi_1 - \cos\phi_2 > \frac{\rho \omega^2 R h^2}{4 \sigma} \quad (\text{A2.16})$$

For equation (A2.13) we now find the following expression.

$$p_1 - p_0 - (h_0 + R(1 - \sin\theta)) \rho g - \frac{\sigma \cos\phi_1}{h(x_1)} - \frac{\sigma \cos\phi_2}{h(x_1)} - \frac{\rho \omega^2 R h(x_1)}{12} = 0 \quad (\text{A2.17})$$

Note : in the results presented in chapter 7, $h_0 = 0$ and $\theta = \pi/2$ were substituted in equation A2.7, thus $p_g = 0$.

APPENDIX A3 : PHYSICAL PROPERTIES FOR THE DYNAMIC FEM MODEL.

Mass of garter spring	$m = 2.75 \cdot 10^{-3}$ [kg]
Initial length of garter spring	$l_0 = 228$ [mm]
Initial spring force	$F_0 = 1.827$ [N]
Garter spring stiffness	$k = 0.108$ [N/m]
Specific mass of seal material (Nitrile)	$\rho = 1.46 \cdot 10^3$ [kg.m ⁻³]

Mooney-Rivlin constants (Nitrile)	$C_1 = -2.746$ [MPa]
	$C_2 = +4.597$ [MPa]

Constants of stress relaxation function $G(t)$ (equation 8.6) have been determined by curve-fits on stress-relaxation tests on Nitrile performed at a strain level $\epsilon = 1$ %. Nitrile exhibits a linear visco-elastic behavior for strain levels $\epsilon < 1.5$ % .

$$G(t) = G_0 + \sum_{i=1}^7 G_i \cdot \exp(-t/\tau_i)$$

$G_0 =$	3.2 [MPa]		
$G_1 =$	3166.7 [MPa]	$\tau_1 =$	0.003 [s]
$G_2 =$	149.7 [MPa]	$\tau_2 =$	0.072 [s]
$G_3 =$	9.9 [MPa]	$\tau_3 =$	1.01 [s]
$G_4 =$	1.03 [MPa]	$\tau_4 =$	19.9 [s]
$G_5 =$	0.43 [MPa]	$\tau_5 =$	367.0 [s]
$G_6 =$	0.39 [MPa]	$\tau_6 =$	3606.0 [s]
$G_7 =$	0.28 [MPa]	$\tau_7 =$	47347.0 [s]

VALUES OF THE PARAMETERS.

$b =$	75 μm
$e =$	10 μm
$p_{\text{cav}} =$	10 kPa
$u_s =$	1.01 mm
$u_d =$	10 μm
$p_s(\xi_3) =$	0.2 MPa
$R =$	35 mm
$\xi_3 =$	18 μm
$\eta =$	0.023 Pa.s

DANKWOORD.

Op deze plaats wil ik alle mensen bedanken die een bijdrage hebben geleverd aan dit proefschrift.

In de eerste plaats bedank ik alle studenten en stagairs die met grote inzet en enthousiasme veel werk verzet hebben en daardoor een belangrijke bijdrage hebben geleverd aan dit proefschrift. Regelmatig wordt in dit proefschrift naar hun werk verwezen.

Prof.Dr.Ir. M.J.W. Schouten en Dr.Ir. G.J.J. van Heijningen hebben waardevolle suggesties gegeven bij het corrigeren van het manuscript. Collega Harry van Leeuwen wil ik bedanken voor de vele interessante discussies en zijn onuitwisbare bijdrage aan de totstandkoming van het VEHD smeringsconcept.

Collega Leon Govaert heeft een zeer belangrijke bijdrage geleverd door zijn onderzoek naar de karakterisering van de materiaal eigenschappen van rubber.

Jan Peels bouwde met groot vakmanschap diverse proefopstellingen en dacht steeds op enthousiaste wijze mee bij de oplossing van constructieve problemen.

Klaas Amersfoort en Rens Kodde zorgden voor een onmisbare ondersteuning op meettechnisch gebied.

De medewerksters van de afdelingsbibliotheek W, Joep Bognetteau-Janssen en Carola Tak wil ik bedanken voor hun vriendelijke assistentie bij het opsporen van literatuur.

Het laatste woord van dank gaat naar mijn ouders, zonder hun inzet zou dit proefschrift niet geschreven zijn.

CURRICULUM VITAE.

- 13-05-1961 Geboren in Totonto, Canada.
- 1973-1979 Gymnasium β , Serviam College, Sittard.
- 1979-1984 Student Werktuigbouwkunde, TU-Eindhoven.
- 1984-1988 Wetenschappelijk assistent, TU-Eindhoven

STELLINGEN BIJ HET PROEFSCHRIFT : "ON THE SEALING AND LUBRICATION MECHANISM OF RADIAL LIP SEALS."

1) Het afdichtmechanisme van radiale lipafdichtingen is gebaseerd op een actieve pompwerking.

- Hoofdstuk 2 van dit proefschrift.

2) De actieve pompwerking van radiale lipafdichtingen wordt gecompenseerd door een capillaire zuigwerking in tegengestelde richting.

- Hoofdstuk 2 van dit proefschrift.

3) De capillaire zuigwerking speelt een belangrijke rol bij het smeringsmechanisme van radiale lipafdichtingen.

- Hoofdstuk 2 van dit proefschrift.

4) Bij de bestudering van het afdichtmechanisme en het smeringsmechanisme van radiale lipafdichtingen heeft een statische beschouwing van de contactcondities slechts een beperkte waarde. In praktijksituaties ontstaat er namelijk een dynamische excitatie van de afdichtingslip ten gevolge van excentriciteiten of onrondheden van de as.

- Hoofdstuk 8 van dit proefschrift.

5) Visco-elastohydrodynamische (VEHD) smering speelt een belangrijke rol bij het smeringsmechanisme van radiale lipafdichtingen.

- Hoofdstuk 8 van dit proefschrift.

6) Ter verhoging van de efficiency en uit didactische overwegingen verdient het aanbeveling om na te gaan welke collegedictaten kunnen worden vervangen door bestaande (Engelstalige) studieboeken.

- College dictaten van afdeling W, TU Eindhoven.

7) Het werktuigbouwkundig ontwerp-kunde-onderwijs aan technische universiteiten krijgt al snel een historisch tintje wanneer studenten wel geleerd wordt om te werken met eenvoudige rekenrecepten (vuistregels, vergeet-me-nietjes, normbladen, veiligheidsfactoren, en nomogrammen), terwijl er tegelijkertijd nauwelijks aandacht wordt besteed aan het praktisch gebruik van moderne CAE (Computer Aided Engineering) technieken.

- "Zelfstudie van de Faculteit Werktuigbouwkunde Technische Universiteit Eindhoven t.b.v. de proefvisitatie-onderwijs." Intern rapport faculteit W, TU Eindhoven, voorjaar 1988.

8) De introductie van CIM (Computer Integrated Manufacturing) in bedrijven is in de eerste plaats een organisatorisch probleem, in de tweede plaats een technisch probleem.

- "CIM : mechanical aspects." ed. By D. Evans. Pergamon Infotech, Frankfurt 1988. (State of the art report 15:7)

9) De geringe populariteit van 'Bebop' muziek kan o.a. verklaard worden uit de hoge informatiestroom-dichtheid van deze muziek en de hoge mate van zelfwerkzaamheid die bij de luisteraar worden verondersteld.

- L. Feather. "Inside Jazz". Da Capo press, New York, 1977.
- "Music and the brain. Studies in the Neurology of Music." ed. by M. Critchly and R.A. Henson. William Heinemann medical books limited, London, 1980.

10) De agressieve dan wel affectieve wijze waarop vele computergebruikers verbaal proberen te communiceren met hun beeldscherm illustreert het onnatuurlijke karakter van informatie-overdracht via een dialoog op basis van strikt formele taal.

- "Technical & Business Communication goes networking: LSP research & applications for the nineties." 2nd Eindhoven Symposium on LSP (Language for special purposes). TU Eindhoven, 3-6 augustus 1988.

11) De samenleving is zodanig ingericht dat een persoon die uitblinkt in een bepaald vak gestimuleerd wordt om leiding te gaan geven aan vakgenoten, met als gevolg dat die persoon aan datgene waarin hij/zij uitblinkt meestal niet meer toekomt.